Space Science Reviews (2024) 220:75
https://doi.org/10.1007/s11214-024-01109-7

Composition and Chemistry of the Martian Atmosphere as Observed by Mars Express and ExoMars Trace Gas Orbiter

Ann C. Vandaele[1] · Shohei Aoki[2] · Sophie Bauduin[3] · Frank Daerden[1] · Anna Fedorova[4] · Marco Giuranna[5] · Oleg Korablev[4] · Franck Lefèvre[6] · Anni Määttänen[6] · Franck Montmessin[6] · Manish R. Patel[7,8] · Michael Smith[9] · Loïc Trompet[1] · Sébastien Viscardy[1] · Yannick Willame[1] · Nao Yoshida[10]

Received: 11 September 2023 / Accepted: 9 September 2024

Abstract

The atmosphere of Mars has been studied for many years now by a long series of missions. The paper focuses on the results obtained by two of these that are led by European researchers overseen by the European Space Agency, i.e., Mars Express which was launched in 2003 and ExoMars Trace Gas Orbiter launched in 2016. Both missions are still providing high-quality data about the atmosphere of Mars, such as abundances of its key species – CO_2, CO, H_2O, O_3 - playing an important role in the different cycles existing on the planet, as well as other trace gases – O_2 (mixing ratio of 3.1 to 5.8 $\times$ 10^{-3} above 90 km), the recently discovered HCl (up to 4 ppbv below 30 km), and the elusive CH_4 (stringent detection limit of 20 pptv). Some instruments are also sensitive enough to provide information on isotopologues of the key elements and have delivered for some of these the first and unique vertical profiles available today ($\delta^{13}C$ and $\delta^{18}O$ in CO_2 and CO, D/H, $\delta^{17}O$ and $\delta^{18}O$ in water vapour). The paper retraces the history of the exploration of the Martian atmosphere putting the results from both missions in perspective.

✉ A.C. Vandaele
a-c.vandaele@aeronomie.be

1 Royal Belgian Institute for Space Aeronomy, Brussels, Belgium

2 Department of Complexity Science and Engineering, Graduate School of Frontier Sciences, The University of Tokyo, 5-1-5 Kashiwanoha, Kashiwa, Chiba 277-8561, Japan

3 Université libre de Bruxelles (ULB), Spectroscopy, Quantum Chemistry and Atmospheric Remote Sensing (SQUARES), Brussels, Belgium

4 Space Research Institute of the Russian Academy of Sciences (IKI), Moscow, Russia

5 Istituto Nazionale di AstroFisica, Istituto di Astrofisica e Planetologia Spaziali, Rome, Italy

6 LATMOS/IPSL, Sorbonne Université, UVSQ Université Paris-Saclay, CNRS, Paris, France

7 School of Physical Sciences, The Open University, Milton Keynes, UK

8 Space Science and Technology Department, Science and Technology Facilities Council,Rutherford Appleton Laboratory, Didcot, UK

9 NASA Goddard Space Flight Center, Greenbelt, MD, USA

10 Tohoku University, Sendai, Japan

Published online: 24 September 2024

Keywords Neutral composition · Planetary atmosphere · Photochemistry · General circulation modelling

1 Introduction

Mars has an atmosphere mainly composed of carbon dioxide (CO_2, 95.1%, Owen et al. 1977; Trainer et al. 2019); this was already observed by pioneering ground-based infrared observations (Kuiper 1950). Still, the low surface pressure of 6.1 mbar and the abundances of the other gases such as molecular nitrogen (N_2) or argon (Ar) remained largely uncertain before the density of the atmosphere was estimated from Mariner 4 and Mariner 9 radio refraction profiles (Kliore et al. 1965). N_2 (2.7%) and Ar (1.9%) abundances were measured *in situ* by analytical methods on Viking landers (Nier et al. 1976) and were refined later by Curiosity (Mahaffy et al. 2013).

Well-established trace species (whose abundance is below 1%) on Mars include molecular oxygen (O_2, 0.14-0.161%, Hartogh et al. 2010; Mahaffy et al. 2013; Trainer et al. 2019), carbon monoxide (CO), water vapour (H_2O) and ozone (O_3). Molecular oxygen was first detected by ground-based high-resolution spectroscopy (Barker 1972; Carleton and Traub 1972). Ground-based Fourier-transform spectroscopy enabled the discovery of CO (Kaplan et al. 1969) and the first observation of the O_2 singlet dayglow, which serves as a proxy for ozone (Noxon et al. 1976). Ozone was first detected in the UV by Mariner 7 (Barth and Hord 1971). Spinrad et al. (1963) reported low amounts of water vapour (3–10 pr. μm) based on measurements of its 0.82-μm weak absorption band. Out of the minor species with a potential biological or volcanic origin, only methane (CH_4) has been reported.

Long-term monitoring by the Mariner 9 and Viking orbiters and landers allowed for the first characterization of seasonal cycles. The Mariner 9 Infrared Interferometer Spectrometer dataset documented the seasonal change of water vapour on Mars. The summer increase of atmospheric water, above 100 precipitable microns (pr. μm) was first observed from Mars 5 orbiter (Moroz and Nadzhip 1975), and its full cycle was monitored during nearly two Mars Year (MY) by the high-dispersion spectrometer Viking MAWD (Mars Atmospheric Water Detector, Jakosky and Farmer 1982). The ozone seasonal cycle and its vertical profile were first observed by the Mariner 9 UV spectrometer (Barth et al. 1973). Brief observations from the Phobos 2 orbiter (1988-89) provided the first terminator profiles of water vapour (Rodin et al. 1997), and the first maps of water vapour and CO (Rosenqvist et al. 1992).

The Viking mission helped to understand and characterise the main climate cycles of Mars, i.e., those of carbon dioxide, water, and dust (Jakosky and Farmer 1982; Martin 1986). By that time the level of understanding of Mars' atmosphere and climate called for continuous synoptic monitoring, similar to the observation of the Earth's atmosphere. Relevant experiments were prepared for two ambitious expeditions to be launched in 1992, Mars Observer (NASA) and Mars 92 (USSR–Russia). The heritage of these two unsuccessful projects in large outlined the following US investigations and the Mars Express (MEx) mission in Europe, which aimed to recover a part of the science that would have been done by Mars 92.

Operated from 1997 to 2004, the Thermal Emission Spectrometer (TES) onboard Mars Global Surveyor (MGS) orbiter opened a new era in atmospheric studies providing a global view of the Martian climate system in much greater detail. TES characterized the temperature structure from the surface to 40–50 km from the inversion of the strong CO_2 band at 15 μm observed in nadir and mapped water vapour column abundance using the 20–40-μm H_2O band. Since 2002, the THEMIS (Thermal Emission Imaging System) infrared radiometer onboard Mars Odyssey has probed the atmosphere delivering data corresponding to an

altitude of ∼25 km. Since 2006, the Mars Climate Sounder (MCS) limb radiometer on Mars Reconnaissance Orbiter (MRO) delivers profiles of temperature and aerosols (dust, water ice clouds) from the surface to 90 km. These datasets (Smith 2002; Kleinbohl et al. 2009; Smith 2009) overlap with MEx measurements (which started in January 2004 and are still ongoing at the time of writing) and often serve as references for comparison.

Two outstanding questions formulated before MEx in the field of atmospheric composition and chemistry were (1) the stability of CO_2 in the atmosphere and its loss to space and (2) the presence of traces of biological or volcanic activity in the Martian atmosphere. The first efforts to model the chemistry of the Martian atmosphere (McElroy and Donahue 1972) faced difficulties in understanding the apparent stability of CO_2, which is readily dissociated by sunlight at wavelengths $\leq$200 nm. The recombination of CO_2 through the elementary reaction

$$CO + O + M \rightarrow CO_2 + M$$

is so slow that it can be neglected with respect to the competing reaction

$$O + O + M \rightarrow O_2 + M$$

where M represents a third body, usually CO_2 on Mars.

This implies that the atmosphere of Mars should contain large amounts of O_2 and CO. However, measurements showed that the atmosphere is remarkably deficient in dissociation products such as CO, O_2, O_3, and O. Early models (McElroy and Donahue 1972; Parkinson and Hunten 1972) found that the recombination of carbon dioxide is catalysed by trace amounts of water through various forms of odd hydrogen (H, OH, HO_2) and demonstrated the importance of H supply at the photodissociation altitudes in escape processes (see for example Lefèvre and Krasnopolsky 2017 for a full description of the catalytic cycles involved). Yet, balancing the carbon dioxide production has proven difficult (Atreya and Blamont 1990; Atreya and Gu 1994; Krasnopolsky 2006) suggesting that heterogeneous chemistry could have an important impact on the composition of the Martian atmosphere. A newer generation of photochemical models (Lefèvre et al. 2004; Moudden and McConnell 2007; Neary and Daerden 2018) called for detailed observations of the Martian atmosphere, as well as simultaneous and collocated measurements of the CO_2 dissociation products (O_3, CO) and water vapour. Such measurements were to be provided by dedicated instruments, primarily SPICAM (SPectroscopy for the Investigation of the Characteristics of the Atmosphere of Mars) and PFS (Planetary Fourier Spectrometer) on MEx, and later by NOMAD (Nadir and Occultation for MArs Discovery) and ACS (Atmospheric Chemistry Suite) on ExoMars Trace Gas Orbiter (TGO).

Several reports of methane detections (Formisano et al. 2004; Krasnopolsky et al. 2004; Mumma et al. 2009; Webster et al. 2015), whose existence remains debated, raised questions about its sources and sinks. The objectives of the next mission to Mars should therefore include the detection and monitoring of methane. However understanding the potential presence of methane would also require a full characterization of the atmosphere, including the observation of other gases like trace gases, water or CO_2 as well as of dust including the possibility to carry out sensitive measurements of isotopic ratios. In 2018, TGO, a dedicated orbiter with sensitive instruments to measure atmospheric trace gases remotely, reached its science orbit. TGO carries six spectrometers covering the spectral range from UV to thermal infrared with high spectral resolution. The particularity of TGO is to follow an orbit optimized for global mapping through nadir observations and for solar occultations sounding the atmosphere with a high spatial resolution.

Solar and stellar occultations are a powerful method to derive high vertical resolution observations. Stellar occultations allow for a wider coverage depending on the positions of

the spacecraft and the star. Solar occultation has the convenience of a very high signal but at the price of constrained measurements at the terminator (the day/night separator). On Mars, solar occultation measurements were first performed by the Phobos 2 Auguste instrument to retrieve vertical profiles of dust, ozone, water vapour, and temperature (Blamont et al. 1989). Later on, occultation observations were carried out by the SPICAM instrument (Bertaux et al. 2006). MEx also hosted the MaRS (Mars Radio Science) experiment (Pätzold et al. 2016) dedicated to radio occultations from the spacecraft to the Earth. The MAVEN (Mars Atmosphere and Volatile Evolution) mission contains two instruments performing occultation measurements: IUVS (Imaging Ultraviolet Spectrograph) which makes stellar occultations (e.g. Gröller et al. 2018) and EUVM (Extreme UltraViolet Monitor) which uses solar occultations (Thiemann et al. 2018). Both instruments can retrieve density and temperature in the upper atmosphere. On TGO, both NOMAD and ACS can perform solar occultations, which are a valuable technique for retrieving the composition of trace gases in atmospheres and assessing stringent detection limits (Korablev et al. 2019; Knutsen et al. 2021; Montmessin et al. 2021; Braude et al. 2022; Trokhimovskiy et al. 2024), as will be shown in the next sections.

Isotopic ratios play a crucial role in understanding planetary atmospheres as they provide valuable constraints on their modelling as well as on their history. In the long term, they can provide insights into the relevance of atmospheric escape to changes in the planet's climate. In the short term, these ratios are shaped by the various physical and chemical processes the molecules undergo in the present-day atmosphere (e.g., condensation and photolysis-induced fractionation). Previous estimates of carbon and oxygen isotopic anomalies in CO_2 from ground-based observations showed predominantly terrestrial values with marginal deviations (Encrenaz et al. 2005). Measurements by the Phoenix lander (Niles et al. 2010) and the Curiosity rover (Mahaffy et al. 2013; Webster et al. 2013b) provided contradictory values. However, highly variable isotopic ratios in atmospheric CO_2 were revealed by ground-based IR heterodyne spectroscopy (Livengood et al. 2020): Morning observations showed $\delta^{18}O$ varying from $-90‰$ to $+70‰$ over a temperature increase from 267 K to 275 K. This was explained by preferential desorption of the heavier molecules at the surface. Moreover, a recent analysis of measurements at Gale Crater by the Tunable Laser Spectrometer (TLS) of the Sample Analysis at Mars (SAM) instrument, also showed that the $\delta^{13}C$ ratio in sedimentary organics was varying a lot, with negative values, i.e., depletion in ^{13}C. One of the explanations suggested that ^{13}C-depleted organics are produced during the photochemical reduction of CO_2 to formaldehyde (House et al. 2022). This chemical transformation involves CO, which is depleted in ^{13}C compared to CO_2 as a result of the photolysis-induced fractionation of CO_2 (Yoshida et al. 2023).

Today the atmosphere of Mars is about five times more enriched in deuterium (D) than Earth's. This led to the hypothesis that Mars once hosted more water than today (Haberle et al. 2017, and references therein). Many measurements of the current isotopic ratio D/H have indicated that D/H shows a strong seasonal and spatial variability (Webster et al. 2013b; Krasnopolsky 2015b; Villanueva et al. 2015; Encrenaz et al. 2016) associated with the fractionation occurring during the condensation and sublimation of the polar caps (Montmessin et al. 2005). Vertical profiles of D/H were recently obtained by TGO instruments (Vandaele et al. 2019; Alday et al. 2021a; Villanueva et al. 2021, 2022).

The $^{18}O/^{16}O$ and $^{17}O/^{16}O$ isotopic ratios in water are similar to Earth's values (Jakosky and Jones 1997), consistent with the existence of a large reservoir mitigating the effect of the loss of oxygen atoms to space. However, the SAM instrument indicated an enrichment in ^{18}O (84‰, Webster et al. 2013b) also observed by ACS (Alday et al. 2019) while ground-based observations pointed to a depletion in the heavy isotopes (Bjoraker et al. 1989).

In this paper, we will describe the composition and the photochemistry of the atmosphere, as they are known today and in light of the many results obtained primarily by instruments on board the two European missions, MEx and TGO. In the following, we provide short descriptions of these instruments restricted on their capacity to monitor the composition of the neutral atmosphere.

SPICAM performs nadir, limb and stellar/solar occultations and is composed of two channels. SPICAM-UV (Bertaux et al. 2006; Montmessin et al. 2017) covers the 115–310 nm range to study ozone through its Hartley absorption band centred at 250 nm. CO_2 is also observed (120-180 nm) and is then used to derive atmospheric density and temperature. While its spectral range encompasses that of molecular oxygen, the detection of the latter is more challenging, as the resolving power of SPICAM isolates marginally O_2 lines and as the O_2 signature overlaps with strong CO_2 absorption features (Sandel et al. 2015). In nadir mode, SPICAM-UV's capability to detect gases is restricted to ozone since the solar spectrum does not extend blueward of 200 nm where CO_2 absorbs. The SPICAM-IR channel (Korablev et al. 2006) covers the 0.9-1.65 μm range with a resolving power $\lambda/\Delta\lambda \geq 1200$ allowing the detection of water vapor (at 1.38 μm) in nadir and solar occultations. The neighbouring CO_2 band at 1.43 μm is used to derive atmospheric density and temperature in solar occultations. The O_2 ($^1\Delta_g$) infrared emission (at 1.27 μm) is detected in nadir or when observing the limb (Fedorova et al. 2006b).

PFS (Formisano et al. 2005) covers a large spectral range in the infrared with the Long Wavelength Channel (LWC) covering the thermal infrared part, from 250 to 1700 cm^{-1}, and the Short Wavelength Channel (SWC) covering the near-infrared, from 1700 to 8200 cm^{-1}. The spectral resolution of both channels is 1.3 cm^{-1} without apodization and is around 1.8 cm^{-1} when Hamming apodization is applied. The instantaneous field of view is about 1.5° for the SWC and 2.7° for the LWC, which correspond to a spatial resolution of, respectively 6.5 km and 11.5 km when PFS is at its pericentre altitude (250 km). PFS can detect several different chemical species in the Martian atmosphere, including water vapour, carbon monoxide and methane. H_2O can be detected from both LWC (Fouchet et al. 2007) and SWC observations (Tschimmel et al. 2008). CO can be retrieved from the SWC in either its fundamental 1-0 band (centred at 2143 cm^{-1}) or its 2-0 band (centred at 4347 cm^{-1}) (Bouche et al. 2021). In PFS SWC spectra, methane is detected by identification of the Q-branch at 3018 cm^{-1} (Formisano et al. 2004). Thermal infrared observations covering the 15-μm CO_2 band can also be used to infer temperature representative of the atmospheric layers (Giuranna et al. 2021).

The OMEGA (Observatoire pour la Minéralogie, l'Eau, les Glaces et l'Activité) instrument (Bibring et al. 2004) obtains images of Mars in a broad spectral range from UV to IR (0.35–5.1 μm). Its spectral resolution varies from ~7 nm in the visible to 14–20 nm in the IR in three spectral channels. OMEGA observes in nadir and at the limb. The visible-near IR (VNIR) channel consists of a single push-broom spectrometer covering the range of 0.38-1.05 μm. The short-wave infrared (SWIR) channel includes fore-optics with a mechanical scanner providing a cross-track scanning of the IFOV and two spectrometers operating at 0.93-2.73 μm and 2.55-5.1 μm. While Targeting primarily surface mineralogy, the OMEGA investigations cover various topics, from measuring the surface pressure in non-saturated CO_2 bands to the content of H_2O, CO or nightglows.

With its three channels, the NOMAD instrument (Vandaele et al. 2018) on board ExoMars TGO covers a wide spectral interval which contains the signatures of many atmospheric constituents. NOMAD-UVIS (200-650 nm; resolution ~1.5 nm, Patel et al. 2017) has been optimized for the measurement of ozone, as well as dust and clouds. NOMAD infrared channels, SO for solar occultation (2.3–4.3 μm; $\lambda/\Delta\lambda \approx 17{,}000$, Thomas et al.

2022b) and LNO for nadir and limb observations (2.3–3.8 μm; $\lambda/\Delta\lambda \approx 10{,}000$, Thomas et al. 2022a), are sensitive to key species of the Martian atmosphere, such as CO_2 (from which temperature can be derived), CO, H_2O, HCl, CH_4 and other organics. NOMAD-SO's high spectral resolution allows for the detection of different isotopologues and the determination of isotopic ratios.

The ACS instrument is composed of three channels covering the range from the near-infrared (0.7 μm) to the thermal infrared (16.7 μm or 600 cm^{-1}) (Korablev et al. 2018). The ACS-NIR channel (0.7-1.7 μm; $\lambda/\Delta\lambda = 20{,}000$–$25{,}000$) operates mostly in solar occultations in ten narrow spectral intervals giving access to spectral bands of CO_2, H_2O, CO, O_2 and to aerosols. In occultations, ACS-MIR (2.3–4.5 μm $\lambda/\Delta\lambda \approx 30{,}000$) resolves single lines and is sensitive to mostly the same set of atmospheric constituents and isotopologues such as NOMAD-SO, with a wider instantaneous spectral coverage, at the expense of less frequent measurements. ACS-TIRVIM observes the emitted radiance from Mars (600–1300 cm^{-1}) and solar occultations ($\sim$1300–5000 cm^{-1}) at a resolution of 1.17 cm^{-1} (with Hamming apodization). So far published TIRVIM products are the temperature structure and aerosols in nadir (Guerlet et al. 2022; Vlasov et al. 2022), aerosols from occultations (Fedorova et al. 2020; Luginin et al. 2020) and CO profiles from occultations (Fedorova et al. 2022).

2 Atmospheric Composition

2.1 Carbon Dioxide (CO_2)

Mars atmosphere is mainly composed of CO_2, with an average mixing ratio of 95.1% (Owen et al. 1977; Mahaffy et al. 2013; Trainer et al. 2019). The Martian CO_2 column density is therefore a good proxy for the total density and pressure. There is an important variation in pressure along the seasons on Mars by up to 30% as CO_2 condenses or sublimates on the polar caps. This variation was already observed in the pressure records from the Viking landers and further observed with the OMEGA imaging spectrometer onboard MEx (Forget et al. 2007). Two maxima occur around solstices and two minima around the equinoxes. The maximum closer to the Southern summer solstice is in phase with Mars perihelion (L_S 251°) and, thus, has a higher amplitude. Also due to the CO_2 seasonal cycle, the CO_2 mixing ratio was found, from measurements done at Gale Crater with the SAM instrument, to vary seasonally by $\pm$1% around the average mixing ratio (Trainer et al. 2019).

CO_2 density profiles were recorded during the entries of different landers such as Mars-6 (Kerzhanovich 1977), Vikings 1 and 2 (Nier and McElroy 1977; Seiff and Kirk 1977), Pathfinder (Magalhses et al. 1999) and the Mars Exploration Rovers (Withers and Smith 2006). Further, *in situ* measurements of total density in the upper atmosphere were carried out or during the aerobraking phases of the Mars Global Surveyor, Mars Odyssey (e.g., Keating et al. 1998; Withers 2006), and the Mars Reconnaissance Orbiter (Tolson et al. 2012). Later, the Neutral Gas and Ion Mass Spectrometer (NGIMS) (Stone et al. 2018) and the accelerometer (Zurek et al. 2017) onboard MAVEN recorded respectively CO_2 density and total density profiles.

SPICAM provided the first detailed observations of CO_2 vertical profiles in the 60–130 km altitude region (Forget et al. 2009). These showed that the seasonal variation of CO_2 density corresponds to the temperature variation in the lower atmosphere, primarily influenced by factors such as dust loading and the solar flux. This was confirmed by current observations performed by IUVS (e.g. Jain et al. 2023) and EUVM (Thiemann et al. 2018)

onboard MAVEN, and by the ACS (Fedorova et al. 2020; Belyaev et al. 2022; Fedorova et al. 2023) and NOMAD (Lopez-Valverde et al. 2022; Trompet et al. 2023a,b) instruments onboard TGO.

Forget et al. (2009) observed an increase in CO_2 density around the Solar Longitude L_S 130° that could be related to a dust event. The comparison between measurements done in MY 28 and in MY 32 showed that the seasonal variation of CO_2 density was more important in MY 28 than in MY 32, which could be correlated with the occurrence of a global dust storm in MY 28 (Fedorova et al. 2018). Similar dust-related variations in the CO_2 density were seen by instruments onboard TGO. For example, limb measurements performed by NOMAD-UVIS in MY 35 between 70 and 150 km showed an increase in the CO_2 density around the perihelion (Aoki et al. 2022a). Increases of CO_2 density during the MY 34 global dust storm, as well as during B and C regional events, were observed both by ACS (Belyaev et al. 2022) and NOMAD (Lopez-Valverde et al. 2022; Trompet et al. 2023a,b).

Ground-based observations of the atmosphere of Mars helped improve the spectroscopy of CO_2 by identifying an unreported band (Villanueva et al. 2008b,a). Recently, new absorption features were discovered in the ACS-MIR spectra within the spectral range containing the strongest methane absorption lines (2900–3300 cm^{-1}). After a thorough analysis, most of the features previously attributed to instrumental artefacts impeding the sensitive search of methane (Korablev et al. 2019) were identified as CO_2 lines absent from spectroscopic databases. The frequencies of 30 observed features matched the theoretically calculated P-, Q-, and R-branches of the magnetic dipole or electro-quadrupole band of the main CO_2 isotopologue (Perevalov et al. 2021). This band, forbidden for electric-dipole absorption, has never been observed or numerically calculated before. The relative depth of the branches suggested its magnetic-dipole nature (Trokhimovskiy et al. 2020). The weaker electric quadrupole system was also found in the ACS spectra (Yachmenev et al. 2021).

2.2 Water Vapour (H_2O and HDO)

The first climatology of water was reported by Jakosky and Farmer (1982) from Viking MAWD nadir observations based on the analysis of the 1.38 μm absorption band of water, that same band that SPICAM later used to probe water vapour column abundances. However, unlike previous missions, MEx carries several instruments capable of tracking the water vapour column evolution as a function of Solar Longitude and latitude. PFS (in the NIR and TIR), as well as OMEGA (NIR), and SPICAM (NIR) performed joint surveys of water vapour (Encrenaz et al. 2005; Fedorova et al. 2006a; Fouchet et al. 2007; Maltagliati et al. 2011b) which were compared by Tschimmel et al. (2008), revealing some disagreements that have long resisted reconciliation attempts. Yet, all instruments agreed on the strong variability that characterizes the water seasonal cycle whose abundance has been observed to vary from <1 to >40 pr-μm.

General Circulation Models (GCM) generally reproduce the observed seasonal water cycle by assuming the permanent water ice cap in the north is the only source of water vapour, from which it sublimates when uncovered from CO_2 ice in northern summer (Montmessin et al. 2004; Navarro et al. 2014; Neary and Daerden 2018; Haberle et al. 2019).

In addition, MEx performed the first systematic profiling of H_2O in solar occultation, complementing the first occultations performed by the short-lived Phobos 2 mission that operated 15 years before MEx (Rodin et al. 1997). Solar occultation measurements by SPICAM (Maltagliati et al. 2011a, 2013; Fedorova et al. 2018, 2021b) have revealed the frequent occurrence of water vapour pressures exceeding the saturation vapour pressure in the Martian atmosphere leading to unexpectedly high water vapour abundances in the middle

atmosphere in particular during global dust storms and in perihelion. This type of observation, which is recognized to optimize the sensitivity to trace gases like water, was chosen to become the main observing mode of the two TGO instruments dedicated to the atmosphere, NOMAD and ACS that outmatch the SPICAM detection performances by several orders of magnitude, allowing the capability to probe the faint HDO lines (Vandaele et al. 2019). NOMAD and ACS can perform daily measurements of water vapour vertical distribution (24 occultations per day at a maximum). They confirmed the general behaviour of water vapour within the Martian atmosphere. Water vapour is confined to relatively low altitude regions (below 10-20 km) during the aphelion period (Aoki et al. 2022b; Fedorova et al. 2023), in contrast to the perihelion period during which the abundance of water vapour in the middle atmosphere is increased (Belyaev et al. 2021; Villanueva et al. 2021). This salient feature of Mars' water vapour is captured by GCMs, allowing the better appraisal of the dynamical and thermal mechanisms at work in controlling this behaviour.

During dust storm episodes, both observations and models show that water vapour in the middle atmosphere is increased both in concentration and in the altitude at which it is still observed (Aoki et al. 2019; Fedorova et al. 2020), as a consequence of higher atmospheric temperature associated with increased meridional circulation. Neary et al. (2020) demonstrated this mechanism of increased vertical water transport during the 2018 global dust storm in a GCM. Supersaturation of water vapour is commonly present at high altitudes during dust storms and during the southern summer period (Fedorova et al. 2020; Brines et al. 2023; Poncin et al. 2022) but is also frequently observed above the aerosol layers (Fedorova et al. 2023). GCMs that include cloud microphysics allowing for supersaturation can reproduce these observations (Vals et al. 2022).

The interested reader is referred to Montmessin et al. (2024) for a more detailed discussion.

2.3 Ozone (O_3)

Ozone is an indirect by-product of CO_2 photolysis, which releases oxygen atoms that recombine with molecular oxygen to form O_3 in a three-body reaction:

1) $O + O_2 + M \rightarrow O_3 + M$

which is most efficient when M is CO_2. The ozone destruction is mainly due to the presence of odd hydrogen radicals (HO_x) which result from water vapour photo-dissociation (Clancy and Nair 1996). O_3 is also photo-dissociated but will eventually recombine in the absence of HO_x. The three main reactions responsible for the ozone destruction are:

2) $H_2O + O \rightarrow OH + O_2$
3) $OH + O \rightarrow H + O_2$
4) $H + O_3 \rightarrow OH + O_2$

As the reactions 2) and 3) are much faster than the ozone formation by 1), they are the dominating reactions in the efficient ozone-destroying cycles catalysed by the HO_x. The HO_x being produced by H_2O, the end result is an anti-correlation between O_3 and water vapour (Clancy and Nair 1996; Lefèvre et al. 2004, 2021; Patel et al. 2021). The short lifetime of ozone in the Martian atmosphere (2-3 hours in the daytime) and its high sensitivity to HO_x, makes it a measurable tracer to monitor the chemistry of HO_x chemistry, which are also highly reactive species and of which OH is a key compound known to stabilize the composition level of CO_2 in the Martian atmosphere by recycling it from its photolysis product CO (McElroy and Donahue 1972; Parkinson and Hunten 1972; Clancy and Nair 1996).

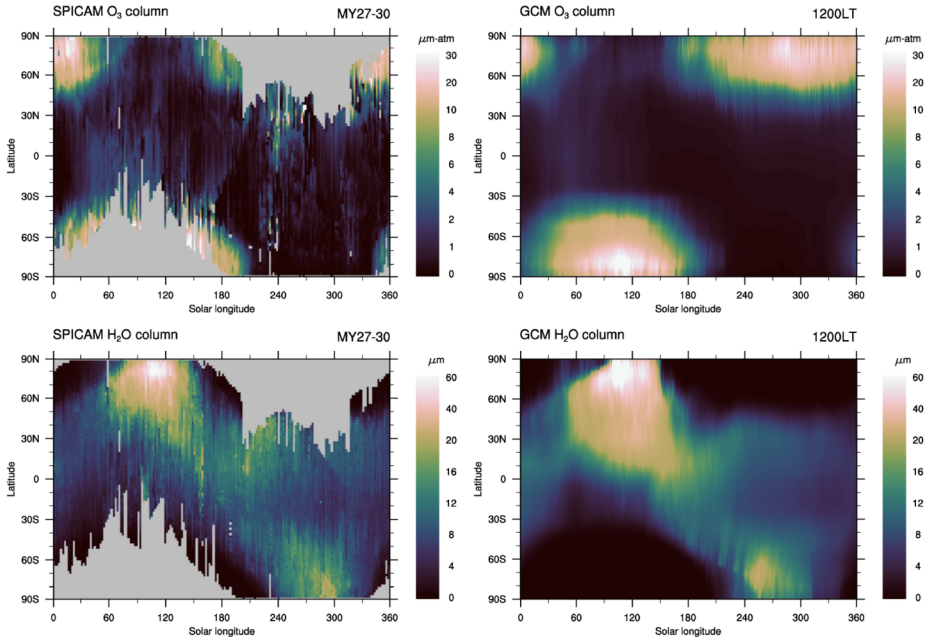

Fig. 1 Climatologies of SPICAM ozone and water vapour as a function of Ls and latitude, compared to the LMD GCM nominal simulation. Left: SPICAM (O_3 top) and H_2O (bottom) column, averaged over MY27–30. The columns are zonally averaged and binned by 2° in Ls and 2° in latitude. Right: LMD GCM nominal simulation of O_3 (top) and H_2O (bottom) calculated at 1200 local time. Units are μm-atm for ozone and pr-μm for water vapour. Figure reproduced from (Lefèvre et al. 2021)

The arrival of MEx around Mars in 2003 brought important contributions to the knowledge of Martian ozone. The first seasonal mapping of ozone over a full Martian year was delivered by Perrier et al. (2006) who derived the total integrated column of O_3 from the SPICAM-UV dayside measurements. The use of a "relative" method, consisting of dividing all the measured spectra by a reference spectrum recorded at the top of Olympus Mons, allowed to compensate for the incomplete knowledge about the instrument's calibration. Note that O_3 nadir observations are sensitive to the lowest part of the atmosphere (typically below ~30 km) where most of the ozone quantity resides. This distribution provided an overview of the ozone cycle whose overall trends and features were generally in good agreement with the model predictions (Lefèvre et al. 2004). Peak O_3 columns are observed at high latitudes in the winter hemisphere when water vapour condenses on the polar caps, whereas low ozone quantities are found during the summer when water vapour abundance is higher again in the atmosphere. At low altitudes, the ozone abundance remains relatively low throughout the year with variations from up to a few μm-atm observed during aphelion to low column values (<1 μm-atm) for the rest of the year (see Fig. 1). The important variability of high ozone columns linked to the polar vortex oscillations was highlighted at the North Pole. Being relatively inert in the polar vortices, ozone acts as a good tracer to study the polar vortex dynamics (Holmes et al. 2017a), which was studied in more detail later with MRO MARCI (Mars Color Imager). Topography-related variations were also reported indicating increases in the ozone column observed in deep basins such as Hellas and Argyre (Clancy et al. 2016).

Willame et al. (2017) investigated a larger set of data of nadir dayside measurements of SPICAM-UV covering 4 Martian years. The retrieval method used was no longer "relative"

as in Perrier et al. (2006). They used an improved calibration and an improved characterization of the aerosol scattering properties for dust and ice clouds. They provided the complete climatology over MY27-30 showing the seasonal pattern and the year-to-year repeatability of the zonally averaged ozone column similar to previous studies. Another re-analysis was performed by Lefèvre et al. (2021) using a similar retrieval method and aerosol parametrization to focus on the O_3 and H_2O relation. The simultaneous observation of ozone and water by SPICAM confirmed the expected anti-correlation at high latitudes, and its absence at low latitudes which was predicted by models (Lefèvre et al. 2004), see Fig. 1. The figure also illustrates the good general agreement between their model and observations. However, the detailed quantitative analysis in Lefèvre et al. (2021) was less satisfactory, as O_3 appears to be underestimated in the models (Lefèvre et al. 2008; Clancy et al. 2016; Daerden et al. 2019; Patel et al. 2021) by about a factor of 2 when using the same H_2O amount as measured. Different assumptions were tested in the model, such as adjusted HO_x kinetics rate or using low-temperature CO_2 cross-sections, but none could solve the discrepancy. The consideration of heterogeneous chemistry brought noticeable improvements at high northern latitudes, due to the adsorption of hydroxyl radicals by ice cloud particles (Brown et al. 2022; Daerden et al. 2023). The general conclusion was that the destruction of O_3 by HO_x appears to be too efficient in the models.

The analysis of the SPICAM-UV stellar occultation measurements (Lebonnois et al. 2006) provided the vertical distribution of night-time ozone between 20-70 km. The observations revealed the presence of two ozone layers, one close to the surface and the second one at higher altitudes. At low and mid-latitudes, the high-altitude layer lies around 40 km and is present from L_S 40° until L_S 130° (see Fig. 2 top and middle right panels). TGO NOMAD observations confirmed the persistence of the high-altitude band of ozone located between approximately 40-50 km as identified by SPICAM and predicted by models (Lefèvre et al. 2004; Daerden et al. 2019, 2022b), particularly prominent in the southern hemisphere and persisting from L_S 0° to 180°At high Southern latitudes, an altitude layer was also detected but with lower concentrations and peaking between 40-60 km altitude (see Fig. 2 bottom right panel). The top of the layer close to the surface could also be observed during southern winter at high latitudes (corresponding to peaks in the ozone column) when the observations could probe below 20 km. A polar altitude layer at about 50 km was also observed by SPICAM above the South pole but not at the North pole (Montmessin and Lefèvre 2013). This polar layer was shown to result from the downward transport of O atoms from the thermosphere by the Hadley circulation. The dichotomy observed between the north and south poles reflects the large orbital variations in the vertical distribution of H_2O. In the perihelion season, due to the high hygropause, the water vapor photolysis produces H atoms in the thermosphere in much larger quantities than in the dry aphelion season. This effect boosts the loss of odd oxygen at high altitudes and prevents the build-up of O_3 quantities as large as in the southern polar region.

The ozone analysis using the SPICAM-UV occultation measurements was performed by Määttänen et al. (2022). This work combines the analysis of both solar and stellar occultations over more than 4 Martian years, representing so far, the longest dataset on O_3 vertical distributions. It extends the previous works of Lebonnois et al. (2006) and Montmessin and Lefèvre (2013) with stellar occultations. Määttänen et al. (2022) also observed the altitude layer present at low-mid latitudes during aphelion (Fig. 2), with concentrations that were shown to be larger at night than at sunrise/sunset, due to photolysis. Comparison with models (Lefèvre et al. 2004) showed a fair overall agreement and similar peak altitudes but highlighted differences in the absolute values of the abundances. A good agreement is also observed between SPICAM and MAVEN IUVS stellar occultations (Gröller et al. 2018).

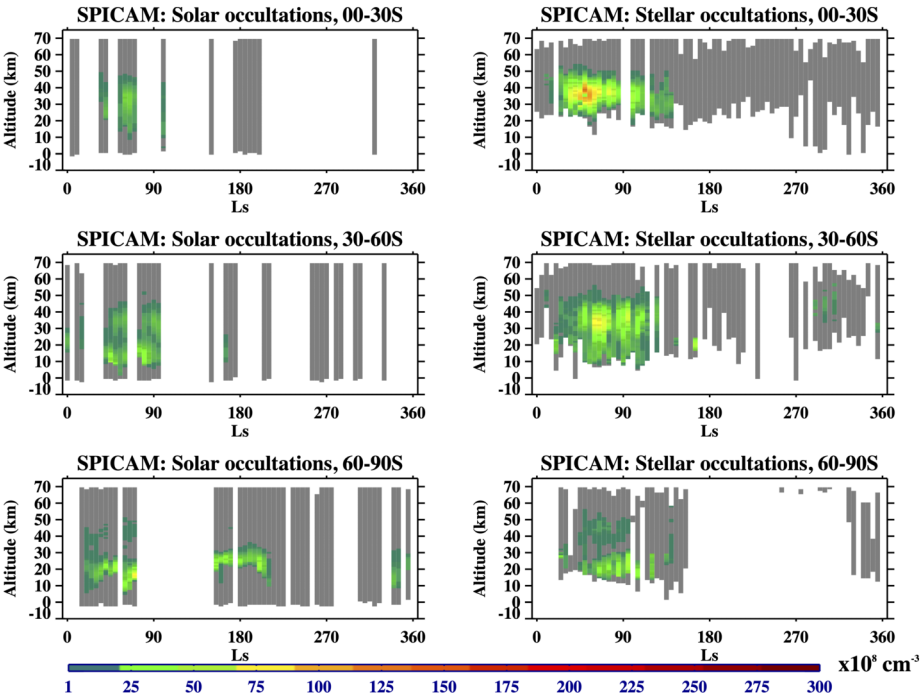

Fig. 2 Ozone concentrations as measured by SPICAM as a function of altitude above the areoid and solar longitude for three latitudinal bands in the southern hemisphere, binned and averaged in a grid of 1 km × 5° Ls. Left: solar occultations. Right: stellar occultations. The colour scale goes from 1 to 300 × 10^8 cm^3 (all values above 300 × 10^8 cm^3 are assigned the same deep red colour). White areas indicate where there were no observational data and gray areas are the ones with data but no confirmed O_3 detection. Figure reproduced from (Määttänen et al. 2022)

IUVS also observed the Southern polar altitude layer but only below 50 km (Fig. 2), i.e., at lower altitudes than predicted by the models.

Following on from SPICAM, the NOMAD-UVIS instrument on TGO continued measurements of the vertical distribution of ozone, through solar occultation measurements. A key advantage of the NOMAD instrument is its ability to simultaneously measure ozone and water vapour concentrations, both in vertical profiles and total column abundance. TGO NOMAD-UVIS measurements of ozone vertical distribution were obtained (Khayat et al. 2021; Patel et al. 2021; Daerden et al. 2022b; Piccialli et al. 2023), showing general agreement with the ozone distribution as observed by SPICAM (Fig. 3) and with models (Khayat et al. 2021; Patel et al. 2021; Daerden et al. 2022b).

During the global dust storm of 2018, NOMAD-UVIS witnessed the wide-spread disappearance of this ozone layer (Daerden et al. 2022b). This phenomenon was also simulated in a GCM which provided insights into the underlying processes involved. The redistribution of water vapour to the middle atmosphere during the dust storm led to the photolytic production of atomic and odd hydrogen species, which, through subsequent reactions reduced the abundances of atomic oxygen. Considering the formation of O_3 by reaction (1), the removal of O immediately results in the suppression of O_3.

By combining observations from the different channels of NOMAD, a comparison of ozone vertical distribution to water vapour was possible for the first time by TGO (Aoki et al.

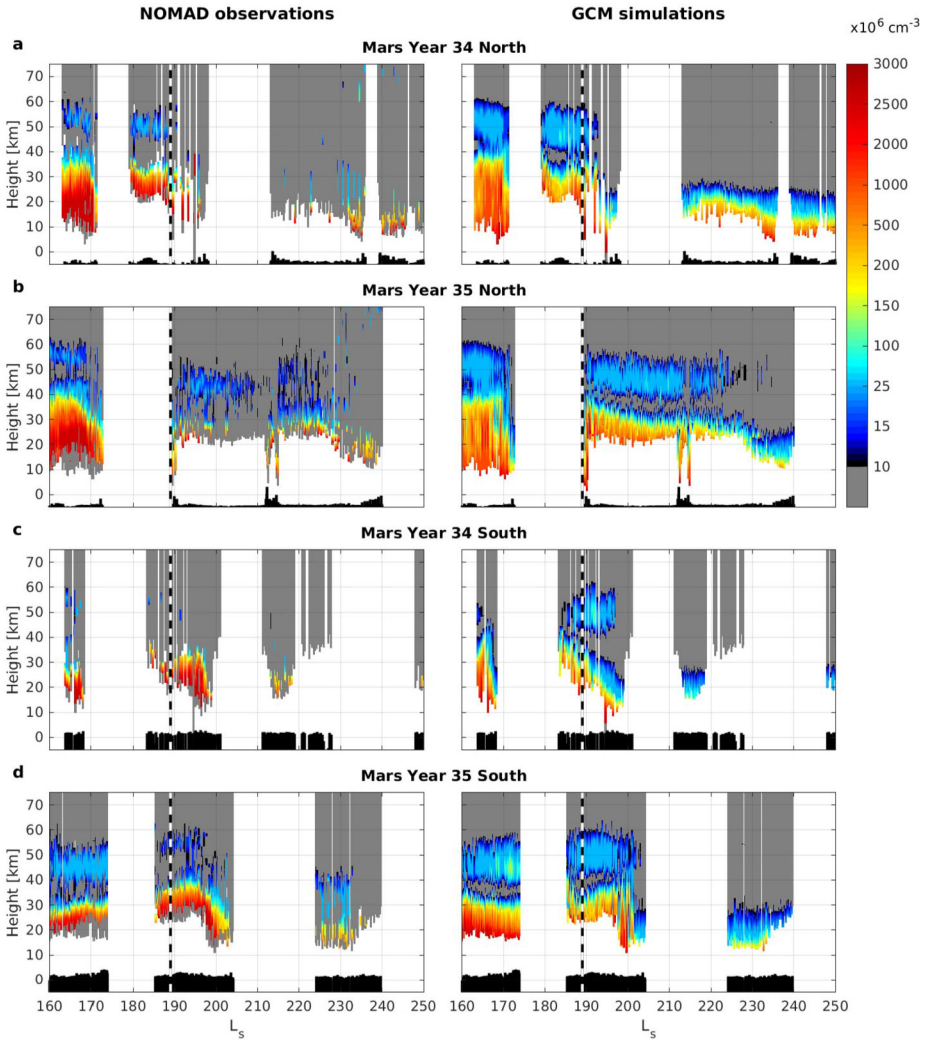

Fig. 3 Time series of the NOMAD-UVIS observed (left) and simulated (right) ozone number density profiles. Panels (a, b) for latitudes north of 45°N, for the same season in MY 34 (a, with GDS) and in Mars year 35 (b). Panels (c, d) show the same for latitudes south of 45°S. Gaps in the data are due to observational restrictions imposed by the orbital geometry of the TGO spacecraft. Grey shading: For the observations, this represents values that were filtered out or are below 10^7 cm^{-3}; for the simulations, values are below 10^7 cm^{-3}. Height is taken with respect to the MOLA reference level (black shading at the bottom of the panels shows the actual surface). Model results were interpolated to the time and location of the observations. The thick vertical dashed lines indicate the onset of the GDS in MY34 and the same time one Mars year later. Figure taken from Daerden et al. (2022b)

2019; Patel et al. 2021), shown in Fig. 4. At perihelion in MY 34 between L_S 200°–320°, O_3 was confined to altitudes below 30 km, with the altitude of peak O_3 values, in general, being coincident with peak H_2O values (Patel et al. 2021). During this period, O_3 and H_2O showed a similar overall correlation in increasing relative abundance with decreasing altitude, demonstrating clearly that while the photochemical anti-correlation of O_3 and water

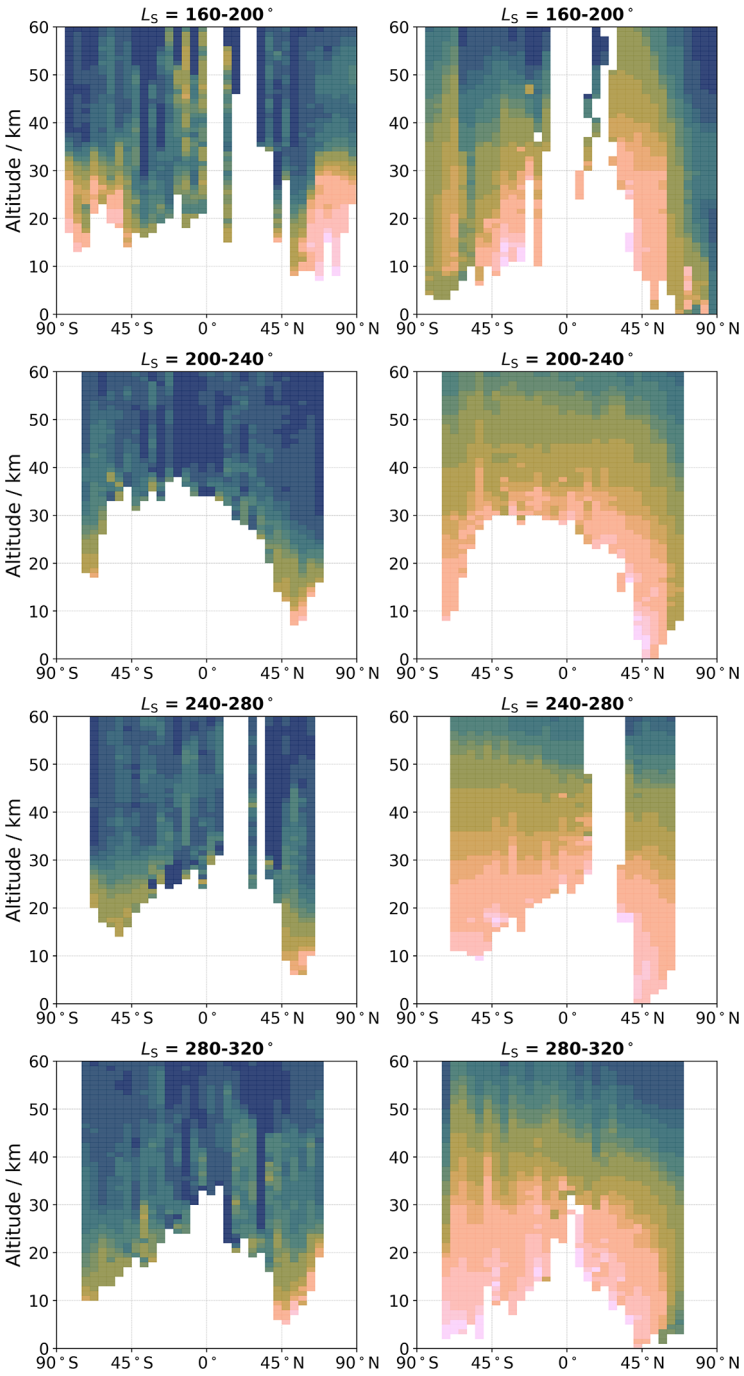

Fig. 4 Latitudinal distribution comparison of (left column) NOMAD O_3 retrievals and (right column) NOMAD H_2O retrievals (Aoki et al. 2019), in Ls intervals of 40° during MY34. Reproduced from Patel et al. (2021)

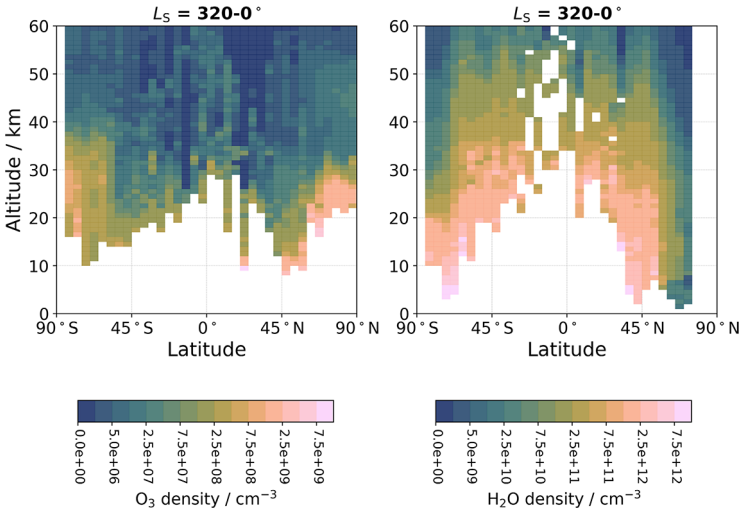

Fig. 4 (*Continued*)

vapour still holds from a chemical perspective, the variation in abundance with altitude is not necessarily anti-correlated. On either side of this period (i.e., L_S 160°–200° and 320°−0°), there were generally lower water vapour concentrations in the atmosphere, and an increase in O_3 abundance was observed at high latitudes in both hemispheres coincident with latitudes where H_2O abundances were decreased, conforming to the classical view of spatial anti-correlation between O_3 and H_2O in their vertical distribution.

Photochemical modelling of Mars ozone has shown that the diurnal variations in ozone are expected to be small with the largest differences expected between the day and night, with larger ozone abundances in the nighttime, associated with the absence of sunlight (Nair et al. 1994; Lefèvre et al. 2004). The amplitude of the day/night difference is highly dependent on latitude and season with daytime ozone column abundances being approximately 4 times smaller than at nighttime at the northern spring equinox and driven by an ozone layer in the middle atmosphere (Lefèvre et al. 2004). The difference in sunrise and sunset terminator O_3 profiles was also highlighted by Patel et al. (2021), with greater abundances often observed in the sunrise profiles.

In terms of variations of O_3 abundance during the daytime, photochemical modelling showed that the largest variations in O_3 can be found in the lowest 3 km of the atmosphere, where the photolysis of NO_2 can result in a mid-morning peak in O_3 (Lefèvre et al. 2021). Recently, Mason et al. (2024) used data from the NOMAD-UVIS channel to characterise the daytime variations in the O_3 total column. To avoid seasonal variations, the diurnal analysis was limited to the northern summer solstice of MY 35. The UVIS O_3 column abundance values show that daytime diurnal variations are generally small (<1 μm), in agreement with modelling results (Lefèvre et al. 2021). The daytime O_3 variations were found to be highly dependent on location and specifically dependent on variations in the higher altitude layers of O_3, when present. In areas with low O_3 abundance, and generally associated with a weak high altitude O_3 layer, the column abundance was found to peak in the mid-morning around 11 local solar time followed by a decay through late morning and the afternoon. The observed mid-morning peak is consistent with the predicted peak in O_3 in the lower atmosphere from the photolysis of NO_2. In regions with a higher O_3 abundance, the O_3 column abundances exhibited a steady increase throughout the day (Mason et al. 2024).

In the spectral range where methane is absorbing, a weak and diffuse infrared ozone band overlapping one of methane's P-branch features was identified. This 003 ← 000 band (3000-3060 cm^{-1}), well-known in the terrestrial atmosphere, has never been seen on Mars before. Observing ozone in the IR solar occultations makes it possible to reconstruct vertical profiles extending from close to the surface (typically 5 km) to 40-50 km (Olsen et al. 2020). As ACS also provides simultaneous measurements of H_2O, the ozone-water vapour anticorrelation has been demonstrated for the lowermost layer of ozone (Olsen et al. 2022).

2.4 Carbon Monoxide (CO)

Carbon monoxide, a minor gas of the Mars atmosphere, is a key constituent of the photochemical carbon cycle and, as such, it plays a crucial role in maintaining the constant abundance of carbon dioxide in Mars atmosphere (Lefèvre and Krasnopolsky 2017). While its formation is due to the photodissociation of carbon dioxide in the upper atmosphere, its direct recombination with the resulting oxygen atoms to recycle CO_2 is spin-forbidden. In the absence of efficient recycling CO_2 processes, this would lead to the rapid build-up of CO and O abundances in the atmosphere. It has been shown that the recombination of CO_2 from CO is catalysed by odd hydrogen radicals (HO_x), formed by the photolysis of water vapour (McElroy and Donahue 1972, see also Lefèvre and Krasnopolsky 2017 for a review of the chemistry involved). Although this catalytic process explains how CO_2 is recycled, it appears however to be too efficient in the models to explain the observed CO abundance. Indeed, photochemical models tend to underestimate CO compared to the observations and this issue is still unresolved today (Lefèvre and Krasnopolsky 2017 and references therein). CO is also a good tracer of atmospheric dynamics given its relatively long lifetime (around 6 years; Krasnopolsky 2007). As a non-condensable gas, its volume mixing ratio (VMR) also shows seasonal variations associated with the seasonal cycle of the surface pressure: enhancements of CO VMR are expected in winter at the poles when CO_2 condenses on the polar caps, while depletions occur in summer when CO_2 sublimates (e.g., Daerden et al. 2019). The spatial and temporal distributions of CO are therefore key to constraining the photochemical and dynamical processes occurring in the Martian atmosphere.

CO has been observed by ground-based facilities (Kaplan et al. 1969; Clancy et al. 1983, 1990; Lellouch et al. 1991; Krasnopolsky 2003). From these observations, its global average abundance was shown to be within 600-800 ppmv (with uncertainties of 25 to 40% depending on the study), and the first investigations of its temporal and spatial variations were conducted. The first clear evidence for a north-south asymmetry in atmospheric CO was reported by Krasnopolsky (2003): During the northern summer, CO decreased by a factor of 1.5 from the southern hemisphere (50°S) to the northern hemisphere. Since then, a more complete picture of spatial and seasonal changes in CO has been obtained from nadir observations, which are dominated by the CO abundances in the lowest scale height of the Martian atmosphere. The exploitation of OMEGA and PFS instruments on board the MEx mission has led to the evaluation of CO seasonal variations respectively over the Hellas Basin (Encrenaz et al. 2006) and at a global scale (Sindoni et al. 2011; Bouche et al. 2021). CO climatologies have also been provided by MRO CRISM (Compact Reconnaissance Imaging Spectrometer for Mars) (Smith et al. 2009, 2018), and more recently, by the NOMAD-LNO spectrometer (Smith et al. 2021).

The first exploitation of a full Martian year of PFS observations was done by Sindoni et al. (2011), who reported a global CO VMR of 990 ± 220 ppmv in agreement with previous studies considering the uncertainties. However, they also reported a significant spread of the retrieved values around this mean, suggesting that CO presents a large variability in

the Martian atmosphere. The authors showed that these variations are strongly bonded to the condensation-sublimation cycle of CO_2, confirming that the CO abundance is strongly decreasing (down to 400 ppmv) during the summer at the polar cap. Their investigation of the relationship between CO and H_2O revealed an anti-correlation. This is explained by the fact that during the winter, both CO_2 and H_2O freeze out. This leads to a decrease of the H_2O VMR but an increase of CO VMR, which is a non-condensable gas. The contrary is observed in spring and summer.

Up to now, the most complete published CO climatology built from PFS observations has been provided by Bouche et al. (2021) based on observations recorded over 7 Martian years (MY 27 to MY 33). Contrary to previous studies which considered averaged spectra to improve the signal-to-noise ratio (SNR), they analysed single SWC spectra. The 1-0 band of CO was used because it is the strongest signature, and also because it is unaffected by the spectral modulation due to mechanical vibrations (Giuranna et al. 2005). Moreover, a series of selection criteria on the atmospheric and surface conditions of observations (e.g., surface temperature, or dust loading) and on the measured radiance level were defined to select spectra with sufficient SNR. Instead of retrieving a column-averaged mixing ratio, a vertical profile of CO was retrieved. Despite the limited vertical resolution of CO profiles obtained by PFS (Bouche et al. 2019; Bauduin et al. 2021), the retrieval process took into account the altitude-dependent vertical sensitivity of the instrument, which is highest at the surface and gradually decreases with altitude, covering an altitude range of 0-20 km.

The global average CO VMR reported by Bouche et al. (2021) is 820 ppmv (with a 25% uncertainty on individual values of CO). This is in very good agreement with ground-based observations (Krasnopolsky 2003, 2015a) and other satellite measurements (Smith et al. 2009; Sindoni et al. 2011; Smith et al. 2018, 2021). Smith et al. (2018) reported similar values using CRISM (mean value of 800 ppmv, uncertainty of 40%) over almost the same period (M Y28-33) while the NOMAD-LNO nadir observation dataset (Smith et al. 2021) covering MY 34-35 gave a mean value of 800 ppmv (uncertainty of 35%). The climatology of the CO vertical distribution on Mars obtained from the combined measurements of the three ACS spectrometers from L_S 163° of MY 34 to the end of MY 35 (Fedorova et al. 2022) gave a mean CO mixing ratio of ~960 ppmv for latitudes between 45°S and 45°N and altitudes below 40 km, still consistent with previous nadir observations even if slightly higher. Similarly, NOMAD-SO solar occultation observations from L_S 160° of MY 34 to L_S 120° of MY 36 (Yoshida et al. 2022) provided a mean value of 726 ppmv for the same latitude range and altitudes between 30 to 45 km.

Figure 5 illustrates the effect of the successive condensation and sublimation of CO_2 at the poles: CO is depleted over the summer poles with a more pronounced effect over the south polar cap. This is explained by the larger CO_2 ice mass that is sublimating from the south polar cap compared to the north. Another difference observed between the two hemispheres is the latitudinal coverage of the CO depletion, extending further equatorward in the Northern Hemisphere (NH) than in the Southern Hemisphere (SH). While the summer CO depletion is well observed, the expected winter pole enhancement is not directly confirmed by any of the three observational datasets presented in Fig. 5 (Smith et al. 2018; Bouche et al. 2021; Smith et al. 2021), although the borders of the north polar enrichment are observed (30-45°N, L_S 180°-315°). At the south pole, the break-up of the polar vortex is clearly observed at L_S 135°-180° (Fig. 5), resulting in the leaking of air rich in CO and transported northward. CO VMRs of 1000 ppmv and above are observed in that period. Model simulations have shown that this CO-enriched air mainly leaks through low-altitude Hellas and Argyre basins before being rapidly transported northward to low latitudes (Smith et al. 2018; Holmes et al. 2019). While the different instruments provide a very similar global behaviour

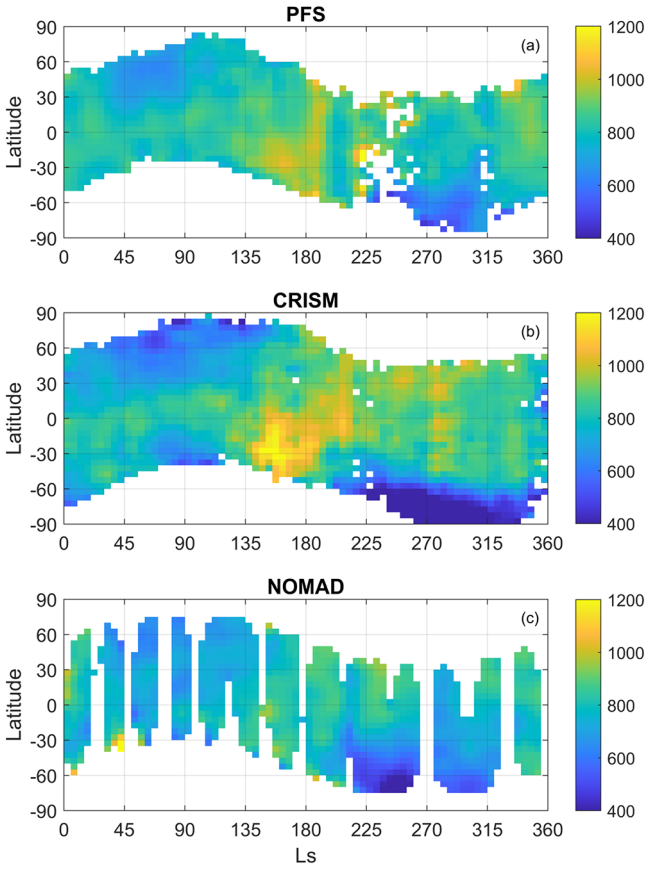

Fig. 5 Seasonal cycle of CO VMR (ppm, colour scale) observed by (a) PFS (Bouche et al. 2021), (b) CRISM (Smith et al. 2018), and (c) NOMAD (Smith et al. 2021). Retrieved CO VMRs have been averaged in 5° × 5° (L_s × latitude) boxes. To better highlight the trends, all distributions have been smoothed following the same method used by Bouche et al. (2021)

of the spatial and seasonal variations of CO, some differences exist in the extension of the depletion of CO at the summer poles and in the intensity of the CO leak following the break of the south polar vortex (Fig. 5). The reason for this difference is not clear and could be due to differences in retrieval approaches. Note finally that none of the instruments could confirm the expected winter polar enhancements as observations in that region are impossible. However, they provide indirect confirmation through the detection of the CO leakage from the South pole and high CO mixing ratios at the borders of north polar enhancements, as explained above.

Discrepancies between the existing CO observational datasets are further discussed in Fig. 6. Panel(a) includes CO column-averaged mixing ratios measured from nadir observations - PFS (Bouche et al. 2021), CRISM (Smith et al. 2018), and NOMAD-LNO (Smith et al. 2021) - and from solar occultations – NOMAD-SO (Yoshida et al. under rev.); ACS-NIR, MIR and TIR (Fedorova et al. 2022). Measurements taken between 45°S and 45°N have been averaged in bins of 5° L_S. For solar occultation measurements, only CO VMRs measured below 40 km for ACS and between 30 and 45 km for NOMAD are taken into

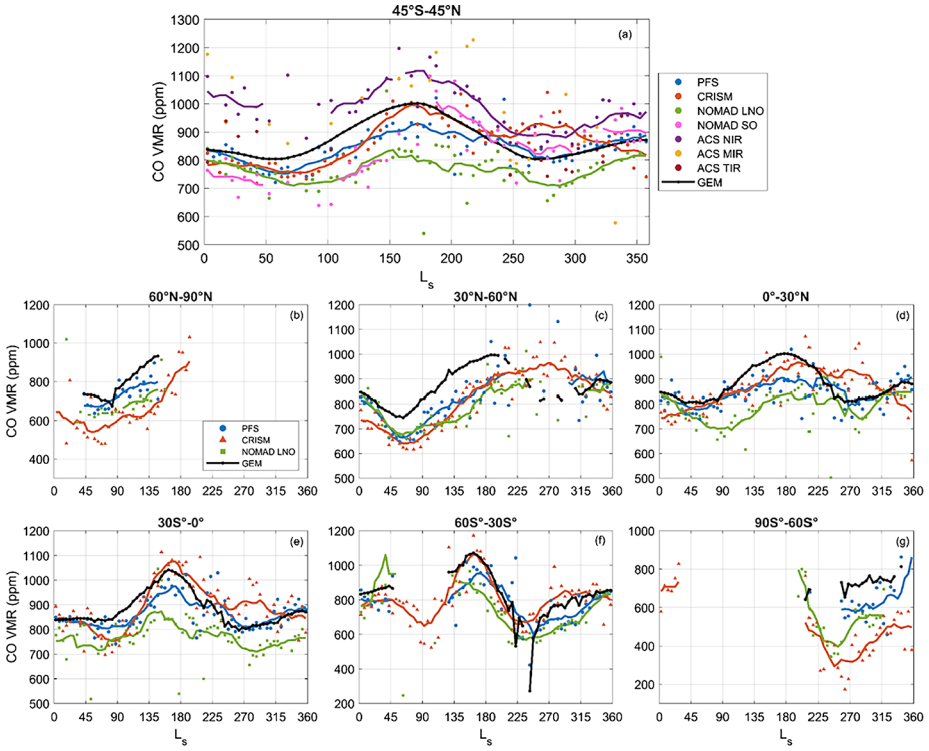

Fig. 6 Comparisons of seasonal CO variations observed by PFS (blue, Bouche et al. 2021), CRISM (orange, Smith et al. 2018), NOMAD-LNO (green, Smith et al. 2021), NOMAD-SO (pink, Yoshida et al. under rev.), ACS (Fedorova et al. 2022): NIR (purple), MIR (yellow) and TIR (dark red) for (Panels b to g) 9 latitude bands and (Panel a) for the 45°S-45°N latitudinal bin. Panels (b) to (g) show the seasonal variations of CO for 6 smaller latitudinal bins and include only nadir observations (PFS, CRISM, NOMAD-LNO). For all panels, retrieved CO VMRs have been averaged in 5° *Ls* boxes. For each instrument (except ACS-MIR and TIR), a moving average (coloured curves) is calculated by sliding a window of 45°. The averages calculated from less than 5 values are not considered. The black curve represents the average CO VMR calculated from GCM simulations (no moving average in this case)

account. All instruments show a very similar behaviour: CO reaches its maximum between L_S 150°-200°, due to the leakage of CO enriched from the South Pole. The instruments seem also to agree in the timings of the CO increase and decrease. In terms of values, the CO VMRs reported by all instruments are in reasonably good agreement considering their respective uncertainties.

Panels (b)-(g) of Fig. 6 show the CO seasonal variations for 6 latitudinal bands. Only nadir observations are included as the number of solar occultation observations is not sufficient to allow a clear representation of the CO seasonal cycle in reduced latitudinal bands. PFS CO VMRs are larger than the other datasets close to the poles, and this is probably due to an overestimation linked to the selection criteria, which favour observations of high CO abundances (Bouche et al. 2021). The timing of the mid and low latitudes CO maximums seems consistent among the three instruments, although it is less obvious from NOMAD-LNO observations. There is a tendency for the maxima to occur later when moving northward. The peak of CO in the NH is more difficult to identify as it seems to spread over a larger range of L_S than in the SH (Smith et al. 2018; Bouche et al. 2021). A CO minimum

is clearly observed by CRISM around L_S 90° at low/mid-SH latitudes and seems to be confirmed by NOMAD-LNO. This minimum is caused by the suppression of CO-enriched air transport from the northern edge of the Hellas basin during the period of CO_2 polar condensation (Holmes et al. 2019). This process maintains the minimum for an extended period while the polar vortex restricts the leakage of CO-enriched air from other longitudes, such as the Argyre basin. The absence of this minimum in the PFS data may be due to the overestimation of PFS CO averages resulting from the selection criteria, which likely excluded the spectra associated with the lowest CO abundances during that period.

While MEx provided only limited information on the vertical profile of CO, solar occultation measurements carried out by NOMAD and ACS have made possible to investigate the global CO vertical distribution in the atmosphere of Mars (Olsen et al. 2021a; Fedorova et al. 2022; Yoshida et al. 2022; Modak et al. 2023; Yoshida et al. under rev.). Using different absorption lines of different intensities, the vertical profile of CO can be reconstructed typically spanning from near the surface up to ∼120 km altitude. TGO observations started in MY 34 (L_S 160°) and are providing a since-then continuous dataset. Interestingly, TGO could observe the onset and subsequent disappearance of a global dust storm, shedding light on its impact on the atmosphere particularly with regard to CO. The typical vertical CO VMR profile is constant below an altitude varying between 60 to 100 km and increases with altitude above due to the photodissociation of CO_2. The predicted enhancement of CO VMR in the middle atmosphere by 3D general circulation models (Lefèvre et al. 2008; Daerden et al. 2019; Holmes et al. 2019) is confirmed by the measurements. The most interesting finding was a strong enrichment of CO near the surface at L_S 100°–200° in high southern latitudes with a layer of 3000–4000 ppmv, corresponding to local depletion of CO_2 (Fedorova et al. 2022). This enrichment was also found at equinoxes above 50 km at high latitudes of both hemispheres. It is explained by the downwelling flux of the Hadley circulation on Mars, which drags the CO-enriched air down to lower altitudes. The comparison with the Mars Planetary Climate Model (PCM) GCM (Fedorova et al. 2022) shows that the model overestimates the intensity of this process, bringing too much CO to the pole. The observed minimum of CO in the high and mid-latitudes southern summer atmosphere amounts to 700–750 ppmv, mostly higher than nadir measurements. This can be explained by the decrease of CO toward the surface, at altitudes unreachable by occultations. The interannual comparison of the CO mixing ratio has been performed for two Martian years at L_S 160°–270° to investigate the effect of the dust storm on CO in the low atmosphere. During the global dust storm of MY 34, when the H_2O abundance peaked, less CO was observed than during the calm MY 35, suggesting an impact of HO_x chemistry on the CO abundance through the reaction $CO + OH \rightarrow CO_2 + H$ (Olsen et al. 2021a). CO number density was found to be larger in the morning terminator than in the evening terminator in the winter hemisphere, which could be due to the transportation by the semi-diurnal tide (Kleinbohl et al. 2013).

During the 2018 global dust storm, a prominent depletion in the CO mixing ratio was observed up to 100 km (Olsen et al. 2021a; Fedorova et al. 2022; Modak et al. 2023; Yoshida et al. under rev.). This could be explained by atmospheric chemistry and/or dynamics. It has been observed that large abundances of water vapour can reach above 100 km during dust storms (e.g., Aoki et al. 2019), which would lead to extra production of HO_x species that efficiently removes CO (Olsen et al. 2021a; Fedorova et al. 2022; Modak et al. 2023). Alternatively, a strong meridional circulation intensified by dust storms could further transport CO into the lower atmosphere and decrease CO abundances at 100 km (Yoshida et al. under rev.).

As already mentioned above, CO is a good tracer of the dynamics of the Martian atmosphere. The latitude-altitude distribution of CO, shown in Fig. 7, reveals its seasonal

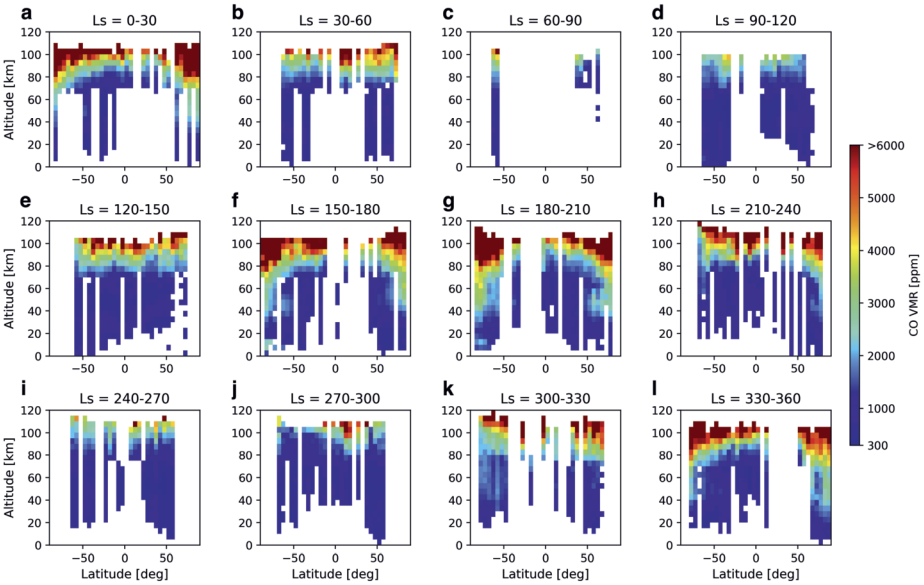

Fig. 7 Seasonal variation of the latitude-altitude distribution of the CO VMR measured in MY 35 and morning terminator (0 - 12 hr) by the NOMAD solar occultation channel. The colour contour represents the CO VMR [ppm]. The dataset is binned into 5 km for altitude and 5 degrees in latitude and 30 degrees for Ls. From (Yoshida et al. under rev.)

variation: From an asymmetric distribution in the mesosphere and lower thermosphere in the equinox season to a symmetric one in the northern winter season. The seasonal variation in the meridional circulation controls the CO distribution in the mesosphere and lower thermosphere, with the CO distribution being symmetric across the equator for the equinoctal seasons, and asymmetric for the solstitial seasons, when higher CO VMRs are found down to lower altitudes over the winter pole (see Daerden et al. 2019, their Fig. 9).

From the CO/CO_2 vertical profiles, it is possible to derive the eddy diffusion coefficient in the Martian middle atmosphere which is a proxy for the vertical transport within the atmosphere (Rodrigo et al. 1990). A detailed analysis showed that the eddy diffusion coefficient increases with altitude, following $K(z) = An(z)^{-1/2}$, where $K(z)$ is the eddy diffusion coefficient, A is constant, and $n(z)$ is the number density. The study also indicated that the amplitude of the eddy diffusion coefficient varies depending on the hemisphere and the season: The estimated eddy diffusion coefficient is larger by a factor of 2 in the southern hemisphere in L_S 240°–270° than that in L_S 90°–120°. The variability of the eddy diffusion coefficient in the northern hemisphere is smaller by a factor of 1.4. This suggests that the efficiency of the vertical diffusion varies with season and hemisphere (Yoshida et al. 2022).

2.5 Methane (CH_4)

Numerous detections reported over the last two decades have garnered significant attention within the scientific community (Formisano et al. 2004; Krasnopolsky et al. 2004; Mumma et al. 2009; Fonti and Marzo 2010; Webster et al. 2015). Several biotic and abiotic mechanisms, with varying degrees of plausibility, have been proposed to explain the origin of the gas (Yung et al. 2018 and references herein).

Photochemical models estimate the lifetime of methane to be around 300 years (Lefèvre and Forget 2009). Accordingly, any ancient methane should have been consumed by now, and its detection would therefore indicate a recent release. Moreover, this gas is expected to exhibit uniform distribution over the planet within a period of two to three months following its emission into the atmosphere (Lefèvre and Forget 2009; Viscardy et al. 2016). However, a significant feature of observed methane concentrations is their substantial temporal and spatial variations.

These variations can only be explained by postulating the existence of a fast removal process, shortening the lifetime of methane by a factor of 1000 or more (Lefèvre and Forget 2009; Mumma et al. 2009; Atreya et al. 2011). This significant inconsistency between the observed and predicted evolution of the gas abundance, together with the potential implications on the atmospheric redox budget, has raised scepticism regarding the reported detections (Zahnle et al. 2011). Moreover, the impact of such a missing mechanism on other well-understood species should be substantial.

The credibility of the detections is mainly supported by the fact that they have been reported by independent groups using different instruments. However, it is important to note that each of these observations has been individually contested, leading to a lack of consensus within the Mars research community. The detections using TES by Fonti and Marzo (2010) have been later considered inconclusive (Fonti et al. 2015). Earth-based telescope observations face challenges such as discriminating between telluric and Martian features, although these concerns have been addressed (Villanueva et al. 2013). Additionally, the detection of methane in only a single spectral feature, along with the limited spectral resolving power and/or SNR of space-borne observations, has raised criticism. *In situ* detections at Gale crater by SAM-TLS on Curiosity have also been strongly questioned (Zahnle 2015; Zahnle and Catling 2019). Additionally, although several mechanisms have been proposed to account for the observed behaviour of the gas abundance (Jensen et al. 2014; Holmes et al. 2015; Zhang et al. 2022), none of them have been deemed convincing due to their inefficiency or unrealistic nature. As a result, doubts about the very existence of Martian methane persist even after two decades of research.

PFS performed more than 600 spot-pointing observations over Gale Crater from Dec. 2012 to July 2021. This observational mode enables the acquisition of several hundred spectra over the same area and in a relatively short period, which can be averaged to increase the SNR. PFS detected methane only once, on 16 June 2013 (Giuranna et al. 2019). The detection of a 15.5 ppbv plume was contemporaneous with a spike of 5.78 ppbv recorded by Curiosity at the crater's floor (Webster et al. 2015) which was initially reported as a non-detection of −2.21 ppbv (Webster et al. 2013a).

In this uncertain context, NOMAD and ACS observations started in April 2018. The gas has never been detected by either of these instruments, and only a stringent upper limit of 20 pptv has been derived from the analysis of hundreds of spectra collected over several years of operation (Korablev et al. 2019; Knutsen et al. 2021; Montmessin et al. 2021).

The main argument put forward to reconcile the methane detections with the TGO upper limit is based on the limited range of TGO observations in solar occultation, which primarily cover the region of the atmosphere above 5 km altitude (Korablev et al. 2019; Montmessin et al. 2021). This limitation thus leaves room for explanations that consider steep vertical gradients of the methane concentration, which would render possible detections by TLS at the surface and by remote-sensing instruments in nadir, while eluding the detection capabilities of the TGO. However, it is worth noting that such explanations do not fully account for the fast atmospheric circulation on Mars, where methane released from the surface is expected to be transported within a few days to higher altitudes that can be effectively probed by the TGO instruments (Viscardy et al. 2016; Holmes et al. 2017b).

A recent model study estimated that a microseepage flux of 1.5×10^{-10} kg m^{-2} sol^{-1} could potentially explain the low methane abundances recorded overnight by SAM-TLS (Moores et al. 2019). Although this flux is extremely low, the region over which emissions at this rate could take place would be limited to a maximum of 0.07% of the planet's surface to remain below the TGO upper limit of 20 pptv. Furthermore, other model investigations identified a potential emission source region northwest of the rover (Luo et al. 2021; Viudez-Moreiras et al. 2021). However, this source would need to be the sole emission site on the entire planet and could not exceed 1.5 millionths of the Martian surface, otherwise violating the TGO upper limit. These findings clearly illustrate the significant constraints imposed on surface emissions by this limit even though the TGO instruments do not directly analyse the air sampled by the rover.

In summary, all the methane detections reported so far have been subject to controversies and criticisms. Moreover, if we assume these detections to be real, the existence of an extremely fast methane removal process must be postulated. However, after two decades of research and several proposed mechanisms in the literature, none of them has been found satisfactory. Additionally, this hypothesis raises more issues than it resolves, particularly considering its implications for well-understood species.

2.6 Other Trace Gases

2.6.1 Molecular Oxygen (O_2)

O_2 was reported by SPICAM in two spectral ranges, corresponding to two distinct forms of O_2. In the UV, it corresponds to O_2 in its fundamental state and thus to its bulk abundance. In that form, it can only be observed in stellar occultation mode above an altitude of 90 km where CO_2 absorption does not fully obstruct the 100 to 200 nm range that contains the O_2 signature. Sandel et al. (2015) derived a mixing ratio varying between 3.1 to 5.8 $\times$ 10^{-3}, matching measurements made by Viking during its atmospheric entry, yet exceeding by a factor of 3 to 4 the values reported for the lower atmosphere where Hartogh et al. (2010) measured 1.4 ($\pm$0.12) $\times$ 10^{-3} (with the Herschel mission) and Trainer et al. (2019) have reported 1.61 ($\pm$0.09) $\times$ 10^{-3} (with SAM on Curiosity). Since then, MAVEN IUVS also achieved O_2 detection with higher resolving power compared to SPICAM-UV and found similar values (Gröller et al. 2015). UV instruments such as SPICAM and IUVS are however unable to tell how much O_2 resides in the lower atmosphere, a gap that ACS is expected to fill thanks to its capability to discriminate the O_2 absorption at 760 nm (Korablev et al. 2018; Fedorova et al. 2021). Altogether, UV and near-IR observations offer access to the O_2 behaviour from the lower to the upper atmosphere of Mars, yielding insights into the main chemical mechanisms controlling its evolution. The Trainer's measurements show a seasonal variation in O_2 that is unexplained by conventional theory and, as with methane, points to a source and/or sink mechanism that has yet to be identified.

The other form of O_2 that SPICAM and OMEGA can detect is produced by O_2 experiencing dissociation through UV photolysis on the dayside or by recombination of atomic oxygen on the nightside, both producing the O_2 ($^1\Delta_g$) emission that has a pronounced peak at 1.27 μm (Fedorova et al. 2006a; Altieri et al. 2009; Fedorova et al. 2012; Guslyakova et al. 2016) and that MRO also detects (Clancy et al. 2017). It does not probe the main O_2 reservoir but serves as a proxy to either gauge the presence of O_3 or to estimate downward atomic fluxes in the middle atmosphere on the night side. Further details on the O_2 ($^1\Delta_g$) emission are given in Gonzalez-Galindo (2024).

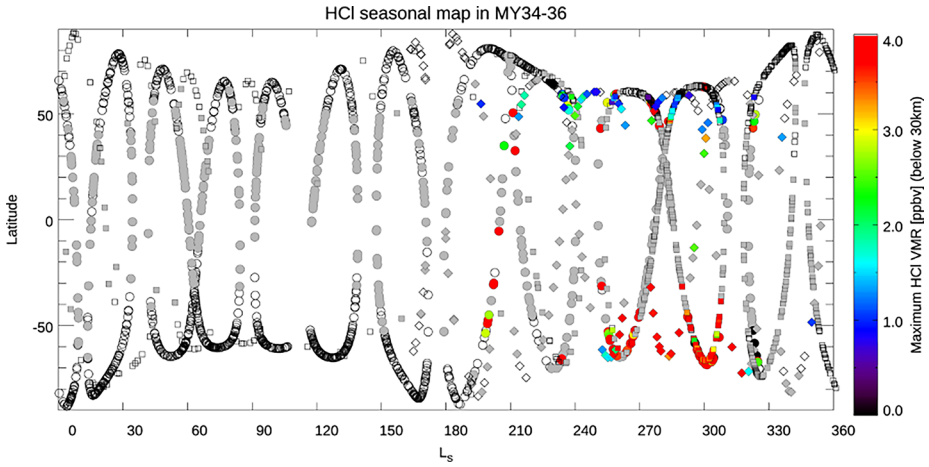

Fig. 8 Seasonal and latitudinal maps of HCl abundances in the atmosphere of Mars (maximum volume mixing ratio below 30 km) in MY 34 (diamond symbols), MY 35 (square symbols), and MY 36 (circular symbols) observed by the NOMAD-SO instrument onboard ExoMars TGO. The x-axis represents the seasons, while the y-axis represents the latitude. The symbols indicate the season/latitude where the NOMAD measurements were performed. White symbols represent non-detections of HCl (<0.3ppb), and grey markers indicate measurements for which a robust analysis could not be performed

2.6.2 Hydrogen Chloride (HCl)

Chlorine plays a key role in the atmospheric chemistry of terrestrial planets. On Earth, trace amounts of chlorine (at the ppb level) result in substantial catalytic depletion of stratospheric ozone (e.g., Solomon 1999). On Venus, chlorine is crucial in the main chemical cycles and is believed to contribute to the stabilization of the dense CO_2 atmosphere (Mahieux et al. 2015). In contrast, ground-based measurements performed during the non-dust storm season on Mars did not reveal the presence of hydrogen chloride (HCl) providing stringent upper limits of 0.2–0.3 ppbv (Villanueva et al. 2007, 2013). The low spectral resolution and sensitivity of instruments onboard MEx prevented the detection of HCl. Consequently, as HCl is expected to be the main reservoir of atmospheric chlorine species (Lefèvre and Krasnopolsky 2017), these upper limits result in such low levels of chlorine atom abundance that chlorine chemistry was considered negligible.

Sensitive solar occultation measurements coupled with the high spectral resolution of the ACS and NOMAD instruments allowed for the recent detection of HCl at the ppb level. Korablev et al. (2021) discovered the transient appearance of HCl in the atmosphere of Mars during the dust storm season (see Fig. 8). Subsequent studies, supported by ground-based observations (Aoki et al. 2024), demonstrated the repetitive nature of this event (Aoki et al. 2021; Olsen et al. 2021c, 2024a). This strong association with the dusty season indicates an interaction between the Martian surface and atmosphere, where airborne dust, containing perchlorate salts ClO_4^- and chloride-bearing minerals Cl^-, could serve as a source of atmospheric chlorine. This would then lead to the rapid production of HCl through the reaction with hydroperoxyl radicals: $Cl + HO_2 \rightarrow HCl + O_2$ (see SI of Aoki et al. 2021). However, the low abundances of measured HCl do not suggest a significant impact of chlorine chemistry on standard species.

The TGO measurements revealed a striking correlation between HCl and H_2O vertical profiles (Aoki et al. 2021; Olsen et al. 2024b). It suggests that the production and destruction

mechanisms of HCl are related to water. One of the key molecules to produce HCl, HO_2, can be produced by photolysis of water vapour. Also, the uptake on water ice cloud particles can temporarily remove HCl from the atmosphere (Luginin et al. 2024).

Soon after the end of the dust storm season, the HCl abundance declines at an unexpectedly high rate that cannot be explained by conventional gas-phase photochemistry (Lefèvre and Krasnopolsky 2017; Aoki et al. 2021). Models involving heterogeneous production of HCl on atmospheric aerosols using odd-hydrogen and its products from H_2O photolysis are able to reproduce the HCl abundances, and main features of the observed seasonal trend balancing against the loss on water ice cloud particles (Krasnopolsky 2022; Streeter et al. 2024; Taysum et al. 2024). However, the relevant reactions have not yet been adequately demonstrated in the Martian atmosphere conditions. Therefore, further investigations will be required to identify not only the mechanism(s) leading to the release of HCl during the dust storm event but also those behind its rapid removal from the atmosphere when this event ends.

Both NOMAD and ACS on TGO also performed measurements of the $H^{37}Cl/H^{35}Cl$ isotopic ratio within the Martian atmosphere (Liuzzi et al. 2021; Trokhimovskiy et al. 2021). They obtained values which are consistent with those in surface materials analysed by the Curiosity rover. These findings, along with the comparison with species of similar molar mass such as argon, suggest that chlorine has not undergone significant escape to space. This observation is consistent with the presence of as-yet-unidentified physicochemical processes, which are responsible for the transient appearance of HCl, retaining chlorine in the lower atmosphere and, in turn, preventing its escape. More generally, the measured HCl isotopic ratio implies that the chlorine reservoirs on Mars have likely not undergone substantial processing since the planet's formation.

2.6.3 Other Trace Gases and Upper Limits

NOMAD and ACS have been optimized for the detection of trace gases (high spectral resolution, high sensitivity). They have been intensively used to look for species present in the atmosphere with very low abundances at the limit of the instruments' detection capabilities. In parallel to the continuous monitoring of methane, several other trace gases related to methane and its potential past or present biological or geological role have been targeted. For example, ethane (C_2H_6) and ethylene (C_2H_4) having shorter lifetimes are suitable tracers of ongoing releases. Knutsen et al. (2021) were unable to firmly detect any ethane or ethylene and provided upper limits of 0.1 ppbv and 0.06 ppbv, which are more stringent values compared to previous investigations (Krasnopolsky 2012; Villanueva et al. 2013).

Phosphine (PH_3), just like methane, has recently been promoted as a potential biomarker in planetary atmospheres (Sousa-Silva et al. 2020). Following the recent claim of its detection on Venus (Greaves et al. 2021), Olsen et al. (2021b) used ACS, which has a spectral range that includes several absorption lines of PH_3, to search for PH_3 in the atmosphere of Mars. No detection was obtained and only upper limits of 0.1–0.6 ppbv could be derived.

The sulphur species (SO_2, H_2S, and OCS) have been searched in the Martian atmosphere by ACS-MIR as a strong indicator of volcanic outgassing from the surface of Mars (Braude et al. 2022). Despite no detection, the upper limits have been determined for SO_2 at 20 ppbv, H_2S at 15 ppbv, and OCS at 0.4 ppbv. For OCS it corresponds to a value lower than any previous upper limits imposed. The obtained upper limits for SO_2 infer that passive volcanic outgassing of this gas must be below 2 ktons/day.

Three nitrogen-bearing species - ammonia (NH_3), hydrogen cyanide (HCN) and cyanoacetylene (HC_3N) - have been also searched by ACS-MIR channel even if they were

not expected to be present in a CO_2-rich Martian atmosphere although outgassing or unknown chemistry sources cannot be discounted. The individual occultation measurements during the warm and dusty perihelion season of MY 36 were analysed and the upper limits of 14, 1.5 and 11 ppbv were obtained for NH_3, HCN and HC_3N respectively (Trokhimovskiy et al. 2024). For ammonia and hydrogen cyanide the upper limits have been improved compared to previously published results. The search for cyanoacetylene on Mars was reported for the first time.

Odd-hydrogen species HO_2 is involved in crucial aspects of the Mars atmospheric chemistry and composition, such as the stability of CO or the underestimation of the O and CO abundances by chemical models. Until recently, there was little observational evidence constraining its abundance. A sensitive search by ACS (Alday et al. 2024) could not identify HO_2 spectral features above the instrument's noise level and was only able to establish an altitude-dependent upper limit of 15 ppbv (5σ) at 10 km, increasing to 100 ppbv at 40 km, improving previous ground-based results by an order of magnitude.

2.7 Isotopic Ratios

NOMAD and ACS on TGO have spectral resolution high enough to distinguish different isotopologues of the main species in the Martian atmosphere, such as CO_2, H_2O, or CO.

ACS measured the abundances of the CO_2 isotopologues $^{12}C^{16}O_2$, $^{13}C^{16}O_2$, $^{18}O^{12}C^{16}O$ and $^{17}O^{12}C^{16}O$ using solar occultation spectra (Alday et al. 2021b). Multiple CO_2 absorption lines were observed over the altitudes from 70 to ∼130 km resulting in the first vertical profiles of O and C isotopes in CO_2. The vertical trends of the isotopic ratios showed heavy isotopes being depleted with increasing altitude, consistent with the expectations from diffusive separation above the homopause at ∼95 km. No significant variations were observed with latitude, season, or local time. The average values below the homopause were close to Earth-like fractionation.

These values are in contradiction with the results obtained by SAM-TLS on the Curiosity rover (Webster et al. 2013b) which indicated an enrichment in the heavy isotopes of CO_2 with respect to Earth's values. Note that the values found by ACS are the results of averaging over many individual profiles obtained under a large range of locations, local times and seasons, while the SAM data correspond to a single location, almost all at the same local time and are therefore probably not representative of the global atmospheric reservoir. Ground-based observations have shown that the isotopic ratios (of $^{18}O/^{16}O$) close to the surface could be highly variable and depended on the surface temperature and surface-atmosphere interaction (Livengood et al. 2020). A similar high variability of the isotopic ratio (of $^{13}C/^{12}C$) was recently also observed in sedimentary organics (House et al. 2022). Moreover, these organics were depleted in ^{13}C, which could be explained by the chemical reduction of CO_2 to formaldehyde through CO. From models, it is indeed expected that CO is depleted in ^{13}C as a follow-up of the photolysis-induced fractionation of CO_2 (Alday et al. 2023; Yoshida et al. 2023). The observed depletion in the sediments would suggest that the organic carbon on early Mars originated from CO (Ueno et al. 2022).

Depletion in ^{13}C in CO was recently confirmed by TGO (Alday et al. 2023; Aoki et al. 2023). Indeed, several isotopologues of CO can be detected with both ACS and NOMAD, from which isotopic ratios in C and O can be derived. Measurements show that the $^{13}C/^{12}C$ ratio is systematically depleted in the heavy isotope with respect to the Earth-like standard. These results confirm that photolysis of CO_2 can lead to a depletion of ^{13}C in CO, which can then be transferred to formaldehyde and other organics which would then accumulate

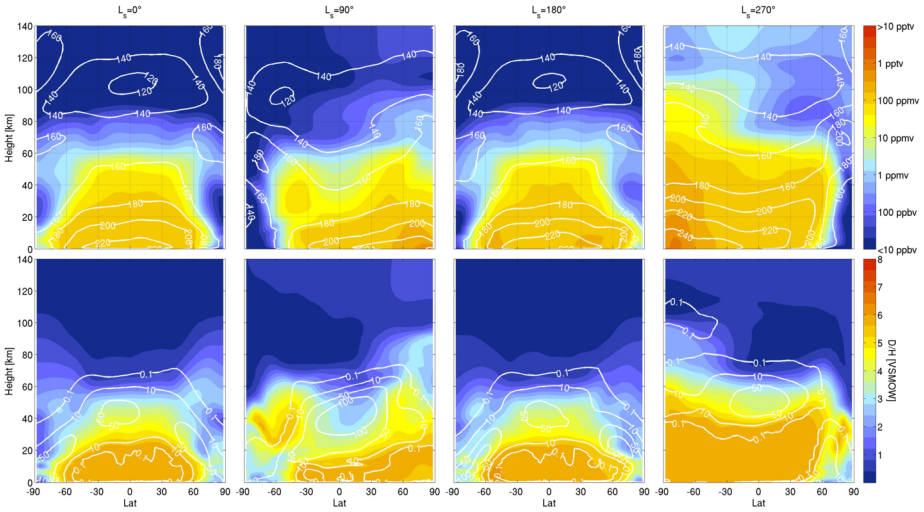

Fig. 9 Latitude-height zonal mean vertical distribution of H_2O (top) and D/H in the gas phase (bottom), as simulated in the GEM-Mars GCM, for four seasons, averaged over all longitudes and local times and over 10 sols. Contours represent the temperature (K, top) and ice water content (ppmv, bottom) as an indication of where clouds form. Figure taken from Daerden et al. (2022a)

on the surface of Mars (House et al. 2022; Ueno et al. 2022). The $^{18}O/^{16}O$ in CO was found to be consistent with the Earth-like fractionation for all latitudes (Alday et al. 2023).

Taking into account the new values of $\delta^{13}C$ in CO_2 to rescale the estimates of total atmospheric loss, the fraction of carbon that escaped to space through history is reduced from 50% (Jakosky 2019) to 20–40% (Alday et al. 2021b) depending on the scenarios considered. This suggests that C losses to space are not as important as previously thought. Moreover, considering the depletion of $\delta^{13}C$ in CO, implies a reduction of the escape fractionation by 25%, suggesting that escape of C through CO photodissociation enriches the atmosphere in ^{13}C more efficiently than previous models indicated. This again means that less escape of C to space is required to explain the current atmospheric state (Alday et al. 2023; Yoshida et al. 2023).

The D/H ratio in water is a good tracer for short-term variation such as the sublimation-condensation process and long-term variation such as atmospheric evolution. D/H ratio in water vapour averaged over the total column of the atmosphere has been investigated by ground-based and space telescopes (Aoki et al. 2015; Villanueva et al. 2015; Encrenaz et al. 2018). They showed that the D/H ratio in the atmosphere of Mars is several times larger than the terrestrial standard value, which can be explained by the preferential escape of H to space over a long period. They also identified spatial anomalies: While lower D/H ratios observed at the high latitudes are attributed to the sublimation-condensation process, some localized anomalies remain unexplained (Villanueva et al. 2015). Investigation of the D/H spatial variation from Mars orbiters is important, however, none of the instruments onboard MEx had the required sensitivity or spectral resolution to do so. Solar occultation measurements with NOMAD and ACS onboard TGO, however, investigated the vertical profile of D/H (Vandaele et al. 2019; Alday et al. 2021a; Villanueva et al. 2021, 2022). As expected by numerical simulations (Montmessin et al. 2005; Rossi et al. 2021; Daerden et al. 2022a), they revealed that the D/H vertical profile decreases at the water ice clouds layer because of the preferential condensation of HDO into water ice. Figure 9 shows the vertical distribu-

tions of water vapour, water ice clouds, and the D/H ratio in water vapour, as simulated in a GCM. The direct connection between vertical decreases in D/H to the presence of water ice clouds is obvious. Model results were extensively compared to NOMAD-SO and ACS-MIR observations of D/H and generally agree very well (Daerden et al. 2022a; Rossi et al. 2022; Vals et al. 2022). These models also confirmed the observed enhancement of the D/H ratio in water vapour up to the middle atmosphere during the 2018 global dust storm.

Variations of the $^{18}O/^{16}O$ in water are expected to be 10 times smaller than the magnitude of the D/H variations, depending on the condensation temperature and the fraction of the condensed water. These estimations are based on the fractionation factor between the ice and vapour phases during condensation and evaporation processes for the D/H and $^{18}O/^{16}O$ ratios from (Merlivat and Nief 1967) and (Majoube 1970) and the assumption of isotopic exchange given by Rayleigh distillation. This was confirmed by measurements of the $\delta^{18}O$ using solar occultation (Alday et al. 2019), which moreover indicated enrichment in both $\delta^{18}O$ ($200 \pm 80\%$) and $\delta^{17}O$ ($230 \pm 110\%$).

3 Conclusions

The paper summarizes the chemical composition and the chemical reactions currently known on Mars based on the latest observations, including those of MEx and TGO instruments. In particular, solar and stellar occultation, which are a powerful tool to derive vertical distributions of many species, contributed to an improved characterization of the atmosphere. These allowed for a more detailed analysis of the relation existing between atmospheric species, as for example between ozone and water vapour. They also provided the first measurement and vertical profiles of HCl, the first vertical profiles of several isotopic ratios ($^{13}C/^{12}C$, $^{17}O/^{16}O$, $^{18}O/^{16}O$, and D/H). Solar occultation is also useful to derive stringent detection limits on many hypothetical trace gases (C_2H_6: 0.1 ppbv, C_2H_4: 0.06 ppbv, CH_4: 20 pptv, PH_3: 0.1–0.6 ppbv, SO_2: 20 ppbv, H_2S: 15 ppbv, OCS: 0.4 ppbv, NH_3: 14 ppbv, HCN: 1.5 ppbv and HC_3N: 11 ppbv).

The seasonal and latitudinal variations of many trace gases of the atmosphere of Mars have been better understood in the last decades thanks to different space missions. Instruments onboard MEx contributed to this effort. Carrying on the measurements, both horizontally and vertically using the observations of NOMAD and ACS instruments, has further improved our knowledge of the different chemical cycles governing the atmosphere of Mars.

Along with the long-term climatologies accumulated by MEx and previous missions, being now complemented by TGO, this huge amount of data describing the 4D behaviour of the Martian atmosphere, has brought new constraints on our understanding of the different processes taking place within the atmosphere. Recent improvements in Mars GCMs benefitted from this considerable amount of data spanning different temporal and spatial scales. Many of the results presented here also demonstrated the benefit of closely interlinking the analysis of the observational data with global modelling.

Although one of the scientific objectives of the ExoMars TGO mission was to provide a final and definitive answer to the methane mystery on Mars, no conclusion can be drawn today based on the many observations performed by the instruments on board. The seeming incompatibility between the observations carried out by MSL and TGO does not allow for a definitive closure to the questions about the presence or not of methane in the planet's atmosphere. Reconciling all measurements is currently unlikely with the available data and probably requires a specific mission to finally resolve the problem. Such a mission should encompass global and continuous coverage to capture the episodic behaviour of methane,

associated with surface-based soil-gas probes and accumulation chambers to evaluate the methane seepage or measure the methane present in the soil (Oehler and Etiope 2017; Yung et al. 2018).

Acknowledgements The NOMAD experiment is led by the Royal Belgian Institute for Space Aeronomy (IASB-BIRA), with Co-PI teams in the United Kingdom (Open University), Spain (IAA-CSIC) and Italy (INAF-IAPS). The PFS experiment was built at the Institute for Space Astrophysics and Planetology (IAPS) of the National Institute for Astrophysics (INAF) and is currently funded by the Italian Space Agency (ASI; agreement number 2018-2-HH.0) in the context of the science activities for the Nadir and Occultation for Mars Discovery spectrometer and the Atmospheric Chemistry Suite onboard the Trace Gas Orbiter ExoMars 2016 and for PFS-MEx. The ACS experiment was built at the Space Research Institute (IKI) in Moscow with assistance of the Laboratoire Atmosphères, Milieux, Observations Spatiales (LATMOS/CNRS) in Paris.

Author Contribution ACV drafted the first version of the review paper. All authors participated in the writing of the content in line with their expertise in the field, and their connection to the missions and instruments described. All authors commented on previous versions of the manuscript. All authors read and approved the final manuscript.

Funding The ACS operations are funded by Roscosmos. The SPICAM experiment was built at the LATMOS and IKI and is being funded by National Centre for Space Studies of France (CNES).

The research leading to these results received funding from The Belgian Science Policy Office (BELSPO) with the financial and contractual coordination by the European Space Agency (ESA) PROgramme de Développement d'EXpériences scientifiques (PRODEX) office (PEA 4000103401, 4000121493), and from the European Union's Horizon 2020 research and innovation programme under grant agreement No 101004052 (RoadMap project). Funding is acknowledged from the UK Space Agency under grants ST/X006549/1, ST/Y000234/1, ST/V005332/1 and ST/V002295/1, from CNES and the Ministry of Science and Education of Russia.

S. Viscardy was supported by the Belgian Science Policy Office BrainBe MICROBE Project. Part of the research was also funded by the F.R.S. FNRS CRAMIC project under grant number T.0171.16. SA is supported by JSPS KAKENHI Grant Numbers 22K03709, 22H05151, 22H00164, and 19H00707.

The authors thank the International Space Science Institute (ISSI) in Bern, Switzerland for the support.

Data Availability All data described and used in the paper are available in public repositories.

All data related to the observations performed by the instruments mentioned in the review can be accessed through the European Space Agency data repository: for the Mars Express mission at https://archives.esac.esa.int/psa/#!Table%20View/Mars%20Express=mission, and for the ExoMars TGO mission at https://archives.esac.esa.int/psa/#!Table%20View/ExoMars%202016=mission.

The results retrieved from the NOMAD measurements used in this article are available at: https://doi.org/10.18758/71021083 (Yoshida et al. under rev.), https://doi.org/10.18758/71021079 (Piccialli et al. 2023), https://doi.org/10.18758/71021076 (Yoshida et al. 2022), https://doi.org/10.18758/71021074 (Trompet et al. 2023a), https://doi.org/10.18758/71021073 (Aoki et al. 2022a), https://doi.org/10.18758/71021072 (Aoki et al. 2022b), https://doi.org/10.18758/71021070 (Daerden et al. 2022b), https://doi.org/10.18758/71021067 (Daerden et al. 2022a), https://doi.org/10.18758/71021066 (Khayat et al. 2021), https://doi.org/10.21954/ou.rd.13580336 (Patel et al. 2021), https://doi.org/10.18758/71021054 (Aoki et al. 2019), https://doi.org/10.18758/71021054 (Neary and Daerden 2018).

The results retrieved from the ACS measurements used in this article are available at: http://doi.org/10.17632/w2b89yr6x5.2 (Fedorova et al. 2022), http://doi.org/10.17632/6xrn9v4dc5.1 (Fedorova et al. 2023) https://doi.org/10.17632/FNGS4KJ27V (Lefèvre et al. 2021) https://github.com/juanaldayparejo/opendata (Alday et al. 2019, 2021a,b, 2023) https://doi.org/10.5287/bodleian:wxxq2m6jo (Olsen et al. 2021a) https://doi.org/10.5287/bodleian:2adpormdz (Olsen et al. 2022) https://doi.org/10.5287/bodleian:aZnnj76MY (Korablev et al. 2021) http://doi.org/10.5287/ora-qmrokgjmr (Olsen et al. 2024b) https://doi.org/10.17632/g6j5t2z73z.2 (Belyaev et al. 2022) https://doi.org/10.17632/995y7ymdgm.1 (Belyaev et al. 2021) https://doi.org/10.17632/35y8775x5z.2 (Vlasov et al. 2022)

The results retrieved from the SPICAM measurements used in this article are available at: http://doi.org/10.17632/vx4gks6bx7.1 (Fedorova et al. 2021) https://doi.org/10.14768/C155973B-C810-4917-B98E-F4D905ED4FC1 (Määttänen et al. 2022) The results retrieved from the PFS measurements used in this article are available at: https://osf.io/xsknv/ (Bouche et al. 2021)

The vertical profiles of ozone, dust, water vapour, carbon dioxide and temperature from the SPICAM and NOMAD instruments are available through the VESPA portal (vespa.obspm.fr). Other derived data are available through VESPA such as datasets from OMEGA, and CRISM as well as datasets from GCMs such as MCD and GEM-Mars.

Declarations

Competing Interests The authors have no relevant financial or non-financial interests to disclose. The authors have no competing interests to declare that are relevant to the content of this article.

References

Alday J, et al (2019) Oxygen isotopic ratios in Martian water vapour observed by ACS MIR on board the ExoMars Trace Gas Orbiter. Astron Astrophys 630:A91. https://doi.org/10.1051/0004-6361/201936234

Alday J, et al (2021a) Isotopic fractionation of water and its photolytic products in the atmosphere of Mars. Nat Astron. https://doi.org/10.1038/s41550-021-01389-x

Alday J, et al (2021b) Isotopic composition of CO_2 in the atmosphere of Mars: fractionation by diffusive separation observed by the ExoMars Trace Gas Orbiter. J Geophys Res, Planets 126:e2021JE006992. https://doi.org/10.1029/2021JE006992

Alday J, et al (2023) Photochemical depletion of heavy CO isotopes in the Martian atmosphere. Nat Astron 7:867–876. https://doi.org/10.1038/s41550-023-01974-2

Alday J, et al (2024) Upper limits of HO_2 in the atmosphere of Mars from the ExoMars Trace Gas Orbiter. Mon Not R Astron Soc 532:4429–4435. https://doi.org/10.1093/mnras/stae1814

Altieri F, et al (2009) O_2 1.27 μm emission maps as derived from OMEGA/MEx data. Icarus 204:499–511

Aoki S, et al (2015) Seasonal variation of the HDO/H_2O ratio in the atmosphere of Mars at the middle of northern spring and beginning of northern summer. Icarus 260:7–22. https://doi.org/10.1016/j.icarus.2015.06.021

Aoki S, et al (2019) Water vapor vertical profiles on Mars in dust storms observed by TGO/NOMAD. J Geophys Res, Planets 124:3482–3497. https://doi.org/10.1029/2019JE006109

Aoki S, et al (2021) Annual appearance of hydrogen chloride on Mars and a striking similarity with the water vapor vertical distribution observed by TGO/NOMAD. Geophys Res Lett 48:e2021GL092506. https://doi.org/10.1029/2021GL092506

Aoki S, et al (2022a) Density and temperature of the upper mesosphere and lower thermosphere of Mars retrieved from the OI 557.7 nm dayglow measured by TGO/NOMAD. J Geophys Res, Planets 127:e2022JE007206

Aoki S, et al (2022b) Global vertical distribution of water vapor on Mars: results from 3.5 years of ExoMars-TGO/NOMAD science operations. J Geophys Res, Planets 127:e2022JE007231. https://doi.org/10.1029/2022JE007231

Aoki S, et al (2023) Depletion of ^{13}C in CO in the atmosphere of Mars suggested by ExoMars-TGO/NOMAD observations. Planet Sci J 4:97. https://doi.org/10.3847/PSJ/acd32f

Aoki S, et al (2024) Global mapping of HCl on Mars by IRTF/iSHELL. Planet Sci J 5:158. https://doi.org/10.3847/PSJ/ad58dc

Atreya SK, Blamont JE (1990) Stability of the Martian atmosphere: possible role of heterogeneous chemistry. Geophys Res Lett 17:287–290

Atreya SK, Gu Z (1994) Stability of the Martian atmosphere: is heterogeneousc catalysis essential? J Geophys Res 99:13133–13145

Atreya SK, et al (2011) Methane on Mars: current observations, interpretation, and future plans. Planet Space Sci 59:133–136

Barker ES (1972) Detection of molecular oxygen in the Martian atmosphere. Nature 238:447–448

Barth CA, Hord CW (1971) Mariner 6 and 7 ultraviolet spectrometer experiment: topography and polar cap. Science 173:197–201

Barth CA, et al (1973) Mariner 9 ultraviolet spectrometer experiment: seasonal variation of ozone on Mars. Science 179:795–796. https://doi.org/10.1126/science.179.4075.795

Bauduin S, et al (2021) Exploiting night-time averaged spectra from PFS/MEX shortwave channel. Part 2: near-surface CO retrievals. Planet Space Sci 199:105188. https://doi.org/10.1016/j.pss.2021.105188
Belyaev D, et al (2021) Revealing a high water abundance in the upper mesosphere of Mars with ACS onboard TGO. Geophys Res Lett 48:e2021GL093411. https://doi.org/10.1029/2021GL093411
Belyaev D, et al (2022) Thermal structure of the middle and upper atmosphere of Mars from ACS/TGO CO2 spectroscopy. J Geophys Res, Planets 127:e2022JE007286. https://doi.org/10.1029/2022JE007286
Bertaux JL, et al (2006) SPICAM on Mars Express: observing modes and overview of UV spectrometer data and scientific results. J Geophys Res 111:E10S90. https://doi.org/10.1029/2006JE002690
Bibring J-P, et al (2004) OMEGA: Observatoire pour la Minéralogie, l'Eau, les Glaces et l'Activité. In: Wilson A, Chicarro A (eds) Mars Express: the scientific payload, ESA SP-1240. ESA Publications Division, Noordwijk, pp 37–49. ISBN 92-9092-556-6
Bjoraker G, et al (1989) Isotopic abundance ratios for hydrogen and oxygen in the Martian atmosphere. Bull Am Astron Soc 21:991
Blamont J, et al (1989) Vertical profiles of dust and ozone in the Martian atmosphere deduced from solar occultation measurements. Nature 341:600–603. https://doi.org/10.1038/341600a0
Bouche J, et al (2019) Retrieval and characterization of carbon monoxide (CO) vertical profiles in the Martian atmosphere from observations of PFS/MEX. J Quant Spectrosc Radiat Transf 238:106498. https://doi.org/10.1016/j.jqsrt.2019.05.009
Bouche J, et al (2021) Seasonal and spatial variability of carbon monoxide (CO) in the Martian atmosphere from PFS/MEX observations. J Geophys Res, Planets 126:e2020JE006480
Braude A, et al (2022) No detection of SO2, H2S, or OCS in the atmosphere of Mars from the first two Martian years of observations from TGO/ACS. Astron Astrophys 658:A86. https://doi.org/10.1051/0004-6361/202142390
Brines A, et al (2023) Water vapor vertical distribution on Mars during perihelion season of MY34 and MY35 with ExoMars-TGO/NOMAD observations. J Geophys Res, Planets 128:e2022JE007273. https://doi.org/10.1029/2022JE007273
Brown MAJ, et al (2022) Impacts of heterogeneous chemistry on vertical profiles of Martian ozone. J Geophys Res, Planets 127:e2022JE007346. https://doi.org/10.1029/2022JE007346
Carleton NP, Traub WA (1972) Detection of molecular oxygen on Mars. Science 177:988–992. https://doi.org/10.1126/science.177.4053.988
Clancy RT, Nair H (1996) Annual (perihelion-aphelion) cycles in the photochemical behavior of the global Mars atmosphere. J Geophys Res 101:12785–12790
Clancy RT, et al (1983) Variability of carbon monoxide in the Mars atmosphere. Icarus 55:282–301
Clancy RT, et al (1990) Global changes in the 0–70 km thermal structure of the Mars atmosphere derived from 1975 to 1989 microwave CO spectra. J Geophys Res 95:14543–14554
Clancy RT, et al (2016) Daily global mapping of Mars ozone column abundances with MARCI UV band imaging. Icarus 266:112–133
Clancy RT, et al (2017) Vertical profiles of Mars 1.27 μm O_2 dayglow from MRO CRISM limb spectra: seasonal/global behaviors, comparisons to LMDGCM simulations, and a global definition for Mars water vapor profiles. Icarus 293:132–156. https://doi.org/10.1016/j.icarus.2017.04.011
Daerden F, et al (2019) Mars atmospheric chemistry simulations with the GEM-Mars general circulation model. Icarus 326:197–224. https://doi.org/10.1016/j.icarus.2019.02.030
Daerden F, et al (2022a) Explaining NOMAD D/H observations by cloud-induced fractionation of water vapor on Mars. J Geophys Res, Planets 127:e2021JE007079. https://doi.org/10.1029/2021JE007079
Daerden F, et al (2022b) Planet wide ozone destruction in the middle atmosphere on Mars during global dust storm. Geophys Res Lett 49:e2022GL098821. https://doi.org/10.1029/2022GL098821
Daerden F, et al (2023) Heterogeneous processes in the atmosphere of Mars and impact on H_2O_2 and O_3 abundances. J Geophys Res, Planets 128:e2023JE008014. https://doi.org/10.1029/2023JE008014
Encrenaz T, et al (2005) Infrared imaging specroscopy of Mars: H_2O mapping and determination of CO_2 isotopic ratios. Icarus 179:43–54
Encrenaz T, et al (2006) Seasonal variations of the Martian CO over Hellas as observed by OMEGA/Mars Express. Astron Astrophys 459:265–270. https://doi.org/10.1051/0004-6361:20065586
Encrenaz T, et al (2016) A map of D/H on Mars in the thermal infrared using EXES aboard SOFIA. Astron Astrophys 586:A62. https://doi.org/10.1051/0004-6361/201527018
Encrenaz T, et al (2018) New measurements of D/H on Mars using EXES aboard SOFIA. Astron Astrophys 612:A112
Fedorova A, et al (2021) CO and O_2 in the Martian atmosphere with ACS NIR onboard TGO. EGU General Assembly 2021, virtual (vEGU21)
Fedorova A, et al (2006a) Mars water vapor abundance from SPICAM IR spectrometer: seasonal and geographic distributions. J Geophys Res 111:E09S08. https://doi.org/10.1029/2006JE002695

Fedorova A, et al (2006b) Observation of O2 1.27 mm dayglow by SPICAM IR: seasonal distribution for the first Martian year of Mars Express. J Geophys Res 111:E09S07. https://doi.org/10.1029/2006JE002694
Fedorova A, et al (2012) The O_2 nightglow in the Martian atmosphere by SPICAM onboard of Mars-Express. Icarus 219:596–608. https://doi.org/10.1016/j.icarus.2012.03.031
Fedorova A, et al (2018) Water vapor in the middle atmosphere of Mars during the 2007 global dust storm. Icarus 300:440–457
Fedorova A, et al (2020) Stormy water on Mars: the distribution and saturation of atmospheric water during the dusty season. Science 367:297–300. https://doi.org/10.1126/science.aay9522
Fedorova A, et al (2021b) Multi-annual monitoring of the water vapor vertical distribution on Mars by SPICAM on Mars Express. J Geophys Res, Planets 126:e2020JE006616. https://doi.org/10.1029/2020JE006616
Fedorova A, et al (2022) Climatology of the CO vertical distribution on Mars based on ACS TGO measurements. J Geophys Res, Planets 127:e2022JE007195. https://doi.org/10.1029/2022JE007195
Fedorova A, et al (2023) A two-Martian years survey of the water vapor saturation state on Mars based on ACS NIR/TGO occultations. J Geophys Res, Planets 128:e2022JE007348. https://doi.org/10.1029/2022JE007348
Fonti S, Marzo GA (2010) Mapping the methane on Mars. Astron Astrophys 512:A51
Fonti S, et al (2015) Revisiting the identification of methane on Mars using TES data. Astron Astrophys 581:A136. https://doi.org/10.1051/0004-6361/201526235
Forget F, et al (2007) Remote sensing of surface pressure on Mars with the Mars Express/OMEGA spectrometer: 1. Retrieval method. J Geophys Res, Planets 112:E08S15. https://doi.org/10.1029/2006JE002871
Forget F, et al (2009) Density and temperatures of the upper Martian atmosphere measured by stellar occultations with Mars Express SPICAM. J Geophys Res 114:E01004
Formisano V, et al (2004) Detection of methane in the atmosphere of Mars. Science 306:1758–1761
Formisano V, et al (2005) The Planetary Fourier Spectrometer (PFS) onboard the European Mars Express mission. Planet Space Sci 53:963–974
Fouchet T, et al (2007) Martian water vapor: Mars Express PFS/LW observations. Icarus 190:32–49
Giuranna M, et al (2005) Calibration of the planetary Fourier spectrometer short wavelength channel. Planet Space Sci 53:975–991
Giuranna M, et al (2019) Independent confirmation of a methane spike on Mars and a source region East of Gale Crater. Nat Geosci 12:326–332. https://doi.org/10.1038/s41561-019-0331-9
Giuranna M, et al (2021) The current weather and climate of Mars: 12 years of atmospheric monitoring by the planetary Fourier spectrometer on Mars Express. Icarus 353:113406. https://doi.org/10.1016/j.icarus.2019.113406
Gonzalez-Galindo F (2024) Aeronomy of Mars. This journal
Greaves JS, et al (2021) Phosphine gas in the cloud decks of Venus. Nat Astron 5:655–664. https://doi.org/10.1038/s41550-020-1174-4
Gröller H, et al (2015) Probing the Martian atmosphere with MAVEN/IUVS stellar occultations. Geophys Res Lett 42:9064–9070. https://doi.org/10.1002/2015GL065294
Gröller H, et al (2018) MAVEN/IUVS stellar occultation measurements of Mars atmospheric structure and composition. J Geophys Res, Planets 123:1449–1483. https://doi.org/10.1029/2017JE005466
Guerlet S, et al (2022) Thermal structure and aerosols in Mars' atmosphere from TIRVIM/ACS onboard the ExoMars Trace Gas Orbiter: validation of the retrieval algorithm. J Geophys Res, Planets 127:e2021JE007062. https://doi.org/10.1029/2021JE007062
Guslyakova S, et al (2016) Long-term nadir observations of the O_2 dayglow by SPICAM IR. Planet Space Sci 122:1–12. https://doi.org/10.1016/j.pss.2015.12.006
Haberle R, et al (2017) The early Mars climate system. Haberle RM, Clancy RT, Forget F, et al (eds). Cambridge University Press, Cambridge
Haberle RM, et al (2019) Documentation of the NASA/Ames legacy Mars global climate model: simulations of the present seasonal water cycle. Icarus 333:130–164. https://doi.org/10.1016/j.icarus.2019.03.026
Hartogh P, et al (2010) Herschel/HIFI observations of Mars: first detection of O_2 at submillimetre wavelengths and upper limits on HCl and H_2O_2. Astron Astrophys 521:L49. https://doi.org/10.1051/0004-6361/201015160
Holmes JA, et al (2015) Analysing the consistency of Martian methane observations by investigation of global methane transport. Icarus 257:23–32. https://doi.org/10.1016/j.icarus.2015.04.027
Holmes J, et al (2017a) On the link between Martian total ozone and potential vorticity. Icarus 282:104–117. https://doi.org/10.1016/j.icarus.2016.10.004
Holmes JA, et al (2017b) The vertical transport of methane from different potential emission types on Mars. Geophys Res Lett 44:8611–8620. https://doi.org/10.1002/2017GL074613
Holmes J, et al (2019) Global analysis and forecasts of carbon monoxide on Mars. Icarus 328:232–245

House CH, et al (2022) Depleted carbon isotope compositions observed at Gale crater, Mars. Proc Natl Acad Sci 119:e2115651119. https://doi.org/10.1073/pnas.2115651119
Jain SK, et al (2023) Thermal structure of Mars' middle and upper atmospheres: understanding the impacts of dynamics and solar forcing. Icarus 393:114703. https://doi.org/10.1016/j.icarus.2021.114703
Jakosky BM (2019) The CO_2 inventory on Mars. Planet Space Sci 175:52–59. https://doi.org/10.1016/j.pss.2019.06.002
Jakosky BM, Farmer CB (1982) The seasonal and global behavior of water vapor in the Mars atmosphere: complete global results of the Viking atmospheric water detector experiment. J Geophys Res 87:2999–3019. https://doi.org/10.1029/JB087iB04p02999
Jakosky BM, Jones J (1997) The history of Martian volatiles. Rev Geophys 35:1–16
Jensen SJ, et al (2014) A sink for methane on Mars? The answer is blowing in the wind. Icarus 236:24–27. https://doi.org/10.1016/j.icarus.2014.03.036
Kaplan L, et al (1969) Carbon monoxide in the Martian atmosphere. Astrophys J 157:187–192
Keating A, et al (1998) The structure of the upper atmosphere of Mars: in situ accelerometer measurements from Mars Global Surveyor. Science 279:1672–1676. https://doi.org/10.1126/science.279.5357.1672
Kerzhanovich VV (1977) Mars 6: improved analysis of the descent module measurements. Icarus 30:1–25. https://doi.org/10.1016/0019-1035(77)90117-8
Khayat AS, et al (2021) ExoMars TGO/NOMAD-UVIS vertical profiles of ozone: part 2: the high-altitude layers of atmospheric ozone. J Geophys Res, Planets 126:e2021JE006834. https://doi.org/10.1029/2021JE006834
Kleinbohl A, et al (2009) Mars Climate Sounder limb profile retrieval of atmospheric temperature, pressure and dust and water ice opacity. J Geophys Res 114:E10006. https://doi.org/10.1029/2009JE003358
Kleinbohl A, et al (2013) The semidiurnal tide in the middle atmosphere of Mars. Geophys Res Lett 40:1952–1959. https://doi.org/10.1002/grl.50497
Kliore A, et al (1965) Occultation experiment: results of the first direct measurement of Mars's atmosphere and ionosphere. Science 149:1243
Knutsen EW, et al (2021) Comprehensive investigation of Mars methane and organics with ExoMars/NOMAD. Icarus 357:114266. https://doi.org/10.1016/j.icarus.2020.114266
Korablev O, et al (2006) SPICAM IR acousto-optic spectrometer experiment on Mars Express. J Geophys Res 111:1–17
Korablev O, et al (2018) The Atmospheric Chemistry Suite (ACS) of three spectrometers for the ExoMars 2016 Trace Gas Orbiter. Space Sci Rev 214:7. https://doi.org/10.1007/s11214-017-0437-6
Korablev O, et al (2019) No detection of methane on Mars from early ExoMars Trace Gas Orbiter observations. Nature 568:517–5250. https://doi.org/10.1038/s41586-019-1096-4
Korablev O, et al (2021) Transient HCl in the atmosphere of Mars. Sci Adv 7:eabe4386. https://doi.org/10.1126/sciadv.abe4386
Krasnopolsky VA (2003) Spectroscopic mapping of Mars CO mixing ratio: detection of North-South asymmetry. J Geophys Res 108:5010. https://doi.org/10.1029/2002JE001926
Krasnopolsky VA (2006) Photochemistry of the Martian atmosphere: seasonal, latitudinal and diurnal variations. Icarus 185:153–170
Krasnopolsky VA (2007) Long-term spectroscopic observations of Mars using IRTF/CSHELL: mapping of O_2 dayglow, CO, and search for CH_4. Icarus 190:93–102
Krasnopolsky VA (2012) Search for methane and upper limits to ethane and SO_2 on Mars. Icarus 217:144–152. https://doi.org/10.1016/j.icarus.2011.10.019
Krasnopolsky VA (2015a) Variations of carbon monoxide in the Martian lower atmosphere. Icarus 253:149–155
Krasnopolsky VA (2015b) Variations of the HDO/H_2O ratio in the Martian atmosphere and loss of water from Mars. Icarus 257:377–386. https://doi.org/10.1016/j.icarus.2015.05.021
Krasnopolsky V (2022) Photochemistry of HCl in the Martian atmosphere. Icarus 374:114807. https://doi.org/10.1016/j.icarus.2021.114807
Krasnopolsky VA, et al (2004) Detection of methane in the Martian atmosphere: evidence for life? Icarus 172:537–547
Kuiper G (1950) Planetary and satellite atmospheres. Rep Prog Phys 13:247–275
Lebonnois S, et al (2006) Vertical distribution of ozone on Mars as measured by SPICAM/Mars Express using stellar occultations. J Geophys Res 111:E09S05. https://doi.org/10.1029/2005JE002643
Lefèvre F, Forget F (2009) Observed variations of methane on Mars unexplained by known atmospheric chemistry and physics. Nature 460:720–723. https://doi.org/10.1038/nature08228
Lefèvre F, et al (2004) Three-dimensional modeling of ozone on Mars. J Geophys Res 109:E07004. https://doi.org/10.1029/2004JE002268
Lefèvre F, et al (2008) Heterogeneous chemistry in the atmosphere of Mars. Nature 454:971–975. https://doi.org/10.1038/nature07116

Lefèvre F, Krasnopolsky V (2017) Atmosphere photochemistry. In: Haberle RM, Clancy RT, Forget F, et al (eds) The atmosphere and climate of Mars. Cambridge University Press, Cambridge, pp 229–294
Lefèvre F, et al (2021) Relationship between the ozone and water vapor columns on Mars as observed by SPICAM and calculated by a global climate model. J Geophys Res, Planets 126:e2021JE006838. https://doi.org/10.1029/2021JE006838
Lellouch E, et al (1991) Mapping of CO millimeter-wave lines in Mars' atmosphere - the spatial variability of carbon monoxide on Mars. Planet Space Sci 39:219–224
Liuzzi G, et al (2021) Probing the atmospheric Cl isotopic ratio on Mars: implications for planetary evolution and atmospheric chemistry. Geophys Res Lett 48:e2021GL092650. https://doi.org/10.1029/2021GL092650
Livengood T, et al (2020) Evidence for diurnally varying enrichment of heavy oxygen in Mars atmosphere. Icarus 335:113387. https://doi.org/10.1016/j.icarus.2019.113387
Lopez-Valverde MA, et al (2022) Martian atmospheric temperature and density profiles during the 1st year of NOMAD/TGO solar occultation measurements. J Geophys Res, Planets 128:e2022JE007278. https://doi.org/10.1029/2022JE007278
Luginin M, et al (2020) Properties of water ice and dust particles in the atmosphere of Mars during the 2018 global dust storm as inferred from the atmospheric chemistry suite. J Geophys Res, Planets 125:e2020JE006419. https://doi.org/10.1029/2020JE006419
Luginin M, et al (2024) Evidence of rapid hydrogen chloride uptake on water ice in the atmosphere of Mars. Icarus 411:115960. https://doi.org/10.1016/j.icarus.2024.115960
Luo Y, et al (2021) Mars methane sources in northwestern Gale crater inferred from back trajectory modeling. Earth Space Sci 8:e2021EA001915. https://doi.org/10.1029/2021EA001915
Määttänen A, et al (2022) Ozone vertical distribution in Mars years 27–30 from SPICAM/MEX UV occultations. Icarus 387:115162. https://doi.org/10.1016/j.icarus.2022.115162
Magalhses J, et al (1999) Results of the Mars pathfinder atmospheric structure investigation. J Geophys Res, Planets 104:8943–8955. https://doi.org/10.1029/1998JE900041
Mahaffy PR, et al (2013) Abundance and isotopic composition of gases in the Martian atmosphere from the Curiosity rover. Science 341:263–266. https://doi.org/10.1126/science.1237966
Mahieux A, et al (2015) Hydrogen Halides measurements in the Venus upper atmosphere retrieved from SOIR on board Venus Express. Planet Space Sci 113(114):264–274. https://doi.org/10.1016/j.pss.2014.12.014
Majoube M (1970) Fractionation factor of ^{18}O between water vapour and ice. Nature 226:1242. https://doi.org/10.1038/2261242a0
Maltagliati L, et al (2011a) Evidence of water vapor in excess of saturation in the atmosphere of Mars. Science 333:1868–1871
Maltagliati L, et al (2011b) Annual survey of water vapor behavior from the OMEGA mapping spectrometer onboard Mars Express. Icarus 213:480–495. https://doi.org/10.1016/j.icarus.2011.03.030
Maltagliati L, et al (2013) Annual survey of water vapor vertical distribution and water–aerosol coupling in the Martian atmosphere observed by SPICAM/MEx solar occultations. Icarus 223:942–962
Martin TZ (1986) Thermal infrared opacity of the Mars atmosphere. Icarus 66:2–21
Mason J, et al (2024) Climatology and diurnal variation of ozone column abundances for 2.5 Mars years as measured by the NOMAD-UVIS spectrometer. J Geophys Res, Planets 129:e2023JE008270. https://doi.org/10.1029/2023JE008270
McElroy MB, Donahue TM (1972) Stability of the Martian atmosphere. Science 177:986–988
Merlivat L, Nief G (1967) Fractionnement isotopique lors des changements d'état solide-vapeur et liquide-vapeur de l'eau à des températures inférieures à 0 °C. Tellus 19:122–127. https://doi.org/10.1111/j.2153-3490.1967.tb01465.x
Modak A, et al (2023) Retrieval of Martian atmospheric CO vertical profiles from NOMAD observations during the 1st year of TGO operations. J Geophys Res, Planets 128:e2022JE007282. https://doi.org/10.1029/2022JE007282
Montmessin F, Lefèvre F (2013) Transport-driven formation of a polar ozone layer on Mars. Nat Geosci 6:930–933. https://doi.org/10.1038/ngeo1957
Montmessin F, et al (2004) Origin and role of water ice clouds in the Martian water cycle as inferred from a general circulation model. J Geophys Res 109:E10004. https://doi.org/10.1029/2004JE002284
Montmessin F, et al (2005) Modeling the annual cycle of HDO in the Martian atmosphere. J Geophys Res 110:E03006. https://doi.org/10.1029/2004JE002357
Montmessin F, et al (2017) SPICAM on Mars Express: a 10 year in-depth survey of the Martian atmosphere. Icarus 297:195–216. https://doi.org/10.1016/j.icarus.2017.06.022
Montmessin F, et al (2021) A stringent upper limit of 20 pptv for methane on Mars and constraints on its dispersion outside Gale crater. Astron Astrophys 650:A140. https://doi.org/10.1051/0004-6361/202140389

Montmessin F, et al (2024) Water cycle and escape. This journal
Moores J, et al (2019) The methane diurnal variation and microseepage flux at Gale crater, Mars as constrained by the ExoMars Trace Gas Orbiter and Curiosity observations. Geophys Res Lett 46:9430–9438. https://doi.org/10.1029/2019GL083800
Moroz V, Nadzhip A (1975) Measurements of water vapour densities on Mars 5 orbiter: preliminary results. Cosm Res 13:28
Moudden Y, McConnell JC (2007) Three-dimensional on-line chemical modeling in a Mars general circulation model. Icarus 188:18–34
Mumma MJ, et al (2009) Strong release of methane on Mars in northern summer 2003. Science 323:1041–1045
Nair H, et al (1994) A photochemical model of the Martian atmosphere. Icarus 111:124–150
Navarro T, et al (2014) Global climate modeling of the Martian water cycle with improved microphysics and radiatively active water ice clouds. J Geophys Res, Planets 119:1479–1495. https://doi.org/10.1002/2013JE004550
Neary L, Daerden F (2018) The GEM-Mars general circulation model for Mars: description and evaluation. Icarus 300:458–476. https://doi.org/10.1016/j.icarus.2017.09.028
Neary L, et al (2020) Explanation for the increase in high altitude water on Mars observed by NOMAD during the 2018 global dust storm. Geophys Res Lett 46:e2019GL084354. https://doi.org/10.1029/2019GL084354
Nier AO, McElroy MB (1977) Composition and structure of Mars' upper atmosphere: results from the neutral mass spectrometers on Viking 1 and 2. J Geophys Res 82:4341–4349
Nier AO, et al (1976) Composition and structure of the Martian atmosphere: preliminary results from Viking 1. Science 193:786–788. https://doi.org/10.1126/science.193.4255.786
Niles P, et al (2010) Stable isotope measurements of Martian atmospheric CO_2 at the Phoenix landing site. Science 329:1334. https://doi.org/10.1126/science.1192863
Noxon JF, et al (1976) Detection of O_2 dayglow emission from Mars and the Martian ozone abundance. Astrophys J 207:1025–1035. https://doi.org/10.1086/154572
Oehler DZ, Etiope G (2017) Methane seapage on Mars: where to look and why. Astrobiology 17:1233–1264. https://doi.org/10.1089/ast.2017.1657
Olsen KS, et al (2020) First detection of ozone in the mid-infrared at Mars: implications for methane detection. Astron Astrophys 639:A141. https://doi.org/10.1051/0004-6361/202038125
Olsen KS, et al (2021a) The vertical structure of CO in the Martian atmosphere from the ExoMars Trace Gas Orbiter. Nat Geosci 14:67–71. https://doi.org/10.1038/s41561-020-00678-w
Olsen KS, et al (2021b) Upper limits for phosphine (PH_3) in the atmosphere of Mars. Astron Astrophys 649:L1. https://doi.org/10.1051/0004-6361/202140868
Olsen KS, et al (2021c) Seasonal reappearance of HCl in the atmosphere of Mars during the Mars year 35 dusty season. Astron Astrophys 647:A161. https://doi.org/10.1051/0004-6361/202140329
Olsen KS, et al (2022) Seasonal changes in the vertical structure of ozone in the Martian lower atmosphere and its relationship to water vapor. J Geophys Res, Planets 127:e2022JE007213. https://doi.org/10.1029/2022JE007213
Olsen KS, et al (2024a) Relationships between HCl, H_2O, aerosols, and temperature in the Martian atmosphere Part I: climatological outlook. J Geophys Res, Planets 129:e2024JE008350. https://doi.org/10.1029/2024JE008350
Olsen KS, et al (2024b) Relationships between HCl, H_2O, aerosols, and temperature in the Martian atmosphere Part II: quantitative correlations. J Geophys Res, Planets 129:e2024JE008351. https://doi.org/10.1029/2024JE008351
Owen T, et al (1977) The composition of the atmosphere at the surface of Mars. J Geophys Res 82:4635–4639
Parkinson TD, Hunten DM (1972) Spectroscopy and aeronomy of O_2 on Mars. J Atmos Sci 29:1380–1390
Patel MR, et al (2017) The NOMAD spectrometer on the ExoMars Trace Gas Orbiter mission: part 2—design, manufacturing and testing of the ultraviolet and visible channel. Appl Opt 56:2771–2782. https://doi.org/10.1364/AO.56.002771
Patel MR, et al (2021) ExoMars TGO/NOMAD-UVIS vertical 1 profiles of ozone: part 1 – seasonal variation and comparison to water. J Geophys Res, Planets 126:e2021JE006837. https://doi.org/10.1029/2021JE006837
Pätzold M, et al (2016) Mars Express 10 years at Mars: observations by the Mars Express radio science experiment (MaRS). Planet Space Sci 127:44–90. https://doi.org/10.1016/j.pss.2016.02.013
Perevalov BV, et al (2021) Magnetic dipole and electric quadrupole absorption in carbon dioxide. J Quant Spectrosc Radiat Transf 259:107408. https://doi.org/10.1016/j.jqsrt.2020.107408
Perrier S, et al (2006) Global distribution of total ozone on Mars from SPICAM/MEX UV measurements. J Geophys Res 11:E09S06. https://doi.org/10.1029/2006JE002681

Piccialli A, et al (2023) Martian ozone observed by TGO/NOMAD-UVIS solar occultation: an intercomparison of three retrieval methods. Earth Space Sci 10:e2022EA002429. https://doi.org/10.1029/2022EA002429
Poncin L, et al (2022) Water vapor saturation and ice cloud occurrence in the atmosphere of Mars. Planet Space Sci 212:105390. https://doi.org/10.1016/j.pss.2021.105390
Rodin A, et al (1997) Vertical distribution of water in the near-equatorial troposphere of Mars: water vapor and clouds. Icarus 125:212–219
Rodrigo R, et al (1990) A non-steady one-dimensional theoretical model of Mars' neutral atmosphere composition between 30 and 200 km. J Geophys Res 95:14795–14910
Rosenqvist J, et al (1992) Minor constituents in the Martian atmosphere from the ISM/Phobos experiment. Icarus 98:254–270. https://doi.org/10.1016/0019-1035(92)90094-N
Rossi L, et al (2021) The effect of the Martian 2018 global dust storm on HDO as predicted by a Mars global climate model. Geophys Res Lett 48:e2020GL090962. https://doi.org/10.1029/2020GL090962
Rossi L, et al (2022) The HDO cycle on Mars: comparison of ACS observations with GCM simulations. J Geophys Res, Planets 127:e2022JE007201. https://doi.org/10.1029/2022JE007201
Sandel B, et al (2015) Altitude profiles of O_2 on Mars from SPICAM stellar occultations. Icarus 252:154–160
Seiff A, Kirk DB (1977) Structure of the atmosphere of Mars in summer at mid-latitudes. J Geophys Res 82:4364–4378. https://doi.org/10.1029/js082i028p04364
Sindoni G, et al (2011) Observations of water vapour and carbon monoxide in the Martian atmosphere with the SWC of PFS/MEX. Planet Space Sci 59:149–162
Smith MD (2002) The annual cycle of water vapor on Mars as observed by the thermal emission spectrometer. J Geophys Res 107:5115. https://doi.org/10.1029/2001JE001522
Smith MD (2009) THEMIS observations of Mars aerosol optical depth from 2002–2008. Icarus 202:444–452
Smith M, et al (2009) Compact reconnaissance imaging spectrometer observations of water vapor and carbon monoxide. J Geophys Res 114:E00D03. https://doi.org/10.1029/2008JE003288
Smith MD, et al (2018) The climatology of carbon monoxide and interannual variation of water vapor on Mars as observed by CRISM and modeled by the GEM-Mars general circulation model. Icarus 301:117–131. https://doi.org/10.1016/j.icarus.2017.09.027
Smith MD, et al (2021) The climatology of carbon monoxide on Mars as observed by NOMAD nadir-geometry observations. Icarus 362:114404. https://doi.org/10.1016/j.icarus.2021.114404
Solomon S (1999) Stratospheric ozone depletion: a review of concepts and history. Rev Geophys 37:275–316. https://doi.org/10.1029/1999RG900008
Sousa-Silva C, et al (2020) Phosphine as a biosignature gas in exoplanet atmospheres. Astrobiology 20:235–268. https://doi.org/10.1089/ast.2018.1954
Spinrad H, et al (1963) The detection of water vapor on Mars. Astrophys J 137:1319–1321
Stone S, et al (2018) Thermal structure of the Martian upper atmosphere from MAVEN NGIMS. J Geophys Res, Planets 123:2842–2867. https://doi.org/10.1029/2018JE005559
Streeter P, et al (2024) Global distribution and seasonality of Martian atmospheric HCl explained through heterogeneous chemistry. Geophys Res Lett. In press
Taysum B, et al (2024) Observed seasonal changes in Martian hydrogen chloride explained by heterogeneous chemistry. Astron Astrophys 687:A191. https://doi.org/10.1051/0004-6361/202449546
Thiemann E, et al (2018) Mars thermospheric variability revealed by MAVEN EUVM solar occultations: structure at aphelion and perihelion and response to EUV forcing. J Geophys Res, Planets 123:2248–2269. https://doi.org/10.1029/2018JE005550
Thomas IR, et al (2022a) Calibration of NOMAD on ESA's ExoMars Trace Gas Orbiter: part 2 – the Limb, Nadir and Occultation (LNO) channel. Planet Space Sci 218:105410. https://doi.org/10.1016/j.pss.2021.105410
Thomas IR, et al (2022b) Calibration of NOMAD on ESA's ExoMars Trace Gas Orbiter: part 1 – the solar occultation channel. Planet Space Sci 218:105411. https://doi.org/10.1016/j.pss.2021.105411
Tolson RA, et al (2012) Atmospheric modeling using accelerometer data during Mars reconnaissance orbiter aerobraking operations. J Spacecr Rockets 45:511–518. https://doi.org/10.2514/1.34301
Trainer M, et al (2019) Seasonal variations in atmospheric composition as measured in Gale Crater, Mars. J Geophys Res, Planets 124:3000–3024. https://doi.org/10.1029/2019JE006175
Trokhimovskiy A, et al (2020) First observation of the magnetic dipole CO2 absorption band at 3.3 μm in the atmosphere of Mars by the ExoMars Trace Gas Orbiter ACS instrument. Astron Astrophys 639:A142. https://doi.org/10.1051/0004-6361/202038134
Trokhimovskiy A, et al (2021) Isotopes of chlorine from HCl in the Martian atmosphere. Astron Astrophys 651:A32. https://doi.org/10.1051/0004-6361/202140916
Trokhimovskiy A, et al (2024) Revised upper limits for abundances of NH_3, HCN and HC_3N in the Martian atmosphere. Icarus 407:115789. https://doi.org/10.1016/j.icarus.2023.115789

Trompet L, et al (2023a) Carbon dioxide retrievals from NOMAD-SO on ESA's ExoMars Trace Gas Orbiter and temperature profiles retrievals with the hydrostatic equilibrium equation. I. Description of the method. J Geophys Res, Planets 128:e2022JE007277. https://doi.org/10.1029/2022JE007277

Trompet L, et al (2023b) Carbon dioxide retrievals from NOMAD-SO on ESA's ExoMars Trace Gas Orbiter and temperature profiles retrievals with the hydrostatic equilibrium equation. II. Temperature variabilities in the mesosphere at Mars terminator. J Geophys Res, Planets 128:e2022JE007279. https://doi.org/10.1029/2022JE007279

Tschimmel M, et al (2008) Investigation of water vapor on Mars with PFS/SW of Mars Express. Icarus 195:557–575. https://doi.org/10.1016/j.icarus.2008.01.018

Ueno Y, et al (2022) Anomalously ^{13}C-depleted organic matter from CO in early Mars atmosphere. https://doi.org/10.21203/rs.3.rs-2312052/v1

Vals M, et al (2022) Improved modeling of Mars' HDO cycle using a Mars' global climate model. J Geophys Res, Planets 127:e2022JE007192. https://doi.org/10.1029/2022JE007192

Vandaele AC, et al (2018) NOMAD, an integrated suite of three spectrometers for the ExoMars trace gas mission: technical description, science objectives and expected performance. Space Sci Rev 214:80. https://doi.org/10.1007/s11214-018-0517-2

Vandaele AC, et al (2019) Martian dust impact on atmospheric H2O and D/H observed by ExoMars Trace Gas Orbiter. Nature 568:517–520. https://doi.org/10.1038/s41586-019-1096-4

Villanueva G, et al (2007) A Sensitive Search for Multiple Biomarker Gases on Mars, and Discovery of a New Band of Isotopic CO2 in the Prime Search Region for Hydrocarbons. DPS, Orlando, FL

Villanueva G, et al (2008a) Discovery of multiple bands of isotopic CO_2 in the prime spectral regions used when searching for CH_4 and HDO on Mars. J Quant Spectrosc Radiat Transf 109:883–894

Villanueva G, et al (2008b) Identification of a new band system of isotopic CO_2 near 3.3 μm: implications for remote sensing of biomarker gases on Mars. Icarus 195:34–44

Villanueva G, et al (2013) A sensitive search for organics (CH_4, CH_3OH, H_2CO, C_2H_6, C_2H_2, C_2H_4), hydroperoxyl (HO_2), nitrogen compounds (N_2O, NH_3, HCN) and chlorine species (HCl, CH_3Cl) on Mars using ground-based high-resolution infrared spectroscopy. Icarus 223:11–27. https://doi.org/10.1016/j.icarus.2012.11.013

Villanueva G, et al (2015) Strong water isotopic anomalies in the Martian atmosphere: probing current and ancient reservoirs. Science 348:218–221

Villanueva G, et al (2021) Water heavily fractionated as it escapes from Mars 1 as revealed by ExoMars/NOMAD. Adv Sci 7:eabc8843

Villanueva G, et al (2022) The deuterium isotopic ratio of water released from the Martian caps as measured with TGO/NOMAD. Geophys Res Lett 49:e2022GL098161. https://doi.org/10.1029/2022GL098161

Viscardy S, et al (2016) Formation of layers of methane in the atmosphere of Mars after surface release. Geophys Res Lett 43:1868–1875. https://doi.org/10.1002/2015GL067443

Viudez-Moreiras D, et al (2021) Constraints on emission source locations of methane detected by Mars Science Laboratory. J Geophys Res, Planets 126:e2021JE006958. https://doi.org/10.1029/2021JE006958

Vlasov P, et al (2022) Martian atmospheric thermal structure and dust distribution during the MY 34 global dust storm from ACS TIRVIM nadir observations. J Geophys Res, Planets 127:e2022JE007272. https://doi.org/10.1029/2022JE007272

Webster C, et al (2013a) Low upper limit to methane abundance on Mars. Science 342:355–357. https://doi.org/10.1126/science.1242902

Webster CR, et al (2013b) Isotope ratios of H, C and O in CO_2 and H_2O of the Martian atmosphere. Science 341:260–263. https://doi.org/10.1126/science.1237961

Webster C, et al (2015) Mars methane detection and variability at Gale crater. Science 347:415–417. https://doi.org/10.1126/science.1261713

Willame Y, et al (2017) Retrieving cloud, dust and ozone abundances in the Martian atmosphere using SPICAM/UV nadir spectra. Planet Space Sci 142:9–25. https://doi.org/10.1016/j.pss.2017.04.011

Withers P (2006) Mars Global Surveyor and Mars Odyssey accelerometer observations of the Martian upper atmosphere during aerobraking. Geophys Res Lett 33:L02201. https://doi.org/10.1029/2005GL024447

Withers P, Smith M (2006) Atmospheric entry profiles from the Mars exploration rovers spirit and opportunity. Icarus 185:133–142

Yachmenev A, et al (2021) Electric quadrupole transitions in carbon dioxide. J Chem Phys 154:211104. https://doi.org/10.1063/5.0053279

Yoshida N, et al (2022) Variations in vertical CO/CO_2 profiles in the Martian mesosphere and lower thermosphere measured by the ExoMars TGO/NOMAD: implications of variations in eddy diffusion coefficient. Geophys Res Lett 49:e2022GL098485. https://doi.org/10.1029/2022GL098485

Yoshida T, et al (2023) Strong depletion of ^{13}C in CO induced by photolysis of CO_2 in the Martian atmosphere, calculated by a photochemical model planetary. Sci J 4:53. https://doi.org/10.3847/PSJ/acc030

Yoshida N, et al (under rev.) Global distribution of carbon monoxide in the Martian atmosphere derived from the ExoMars-TGO/NOMAD measurement and interpretation with the GEM-Mars model. J Geophys Res, Planets

Yung YL, et al (2018) Methane on Mars and habitability: challenges and responses. Astrobiology 19:1221–1242. https://doi.org/10.1089/ast.2018.1917

Zahnle K (2015) Play it again. J Assam Sci Soc 347:370–371. https://doi.org/10.1126/science.aaa3687

Zahnle K, Catling D (2019) The Paradox of Mars Methane, LPI Contrib. No. 2089, Abs. 6132 (2019). Ninth International Conference on Mars, Pasadena, California

Zahnle K, et al (2011) Is there methane on Mars? Icarus 212:493–503

Zhang X, et al (2022) Reaction of methane and UV-activated perchlorate: relevance to heterogeneous loss of methane in the atmosphere of Mars. Icarus 376:114832. https://doi.org/10.1016/j.icarus.2021.114832

Zurek RW, et al (2017) Mars thermosphere as seen in MAVEN accelerometer data. J Geophys Res Space Phys 122:3798–3814. https://doi.org/10.1002/2016JA023641